NETWORKS AND HETEROGENEOUS MEDIA
©American Institute of Mathematical Sciences
Volume **7**, Number **4**, December **2012**
doi:10.3934/nhm.2012.7.705
pp. **705–740**

A LINK BETWEEN MICROSCOPIC AND MACROSCOPIC MODELS OF SELF-ORGANIZED AGGREGATION

Tadahisa Funaki

Graduate School of Mathematical Sciences, The University of Tokyo
3-8-1 Komaba, Meguro-ku
Tokyo 153-8914, Japan

Hirofumi Izuhara and Masayasu Mimura

Meiji Institute for Advanced Study of Mathematical Sciences, Meiji University
1-1-1 Higashimita, Tamaku, Kawasaki
Kanagawa 214-8571, Japan

Chiyori Urabe

FIRST, Aihara Innovative Mathematical Modelling Project
Japan Science and Technology Agency
Collaborative Research Center for Innovative Mathematical Modelling
Institute of Industrial Science, The University of Tokyo
4-6-1 Komaba, Meguro-ku, Tokyo 153-8505, Japan

Abstract. In some species, one of the roles of pheromones is to influence aggregation behavior. We first propose a macroscopic cross-diffusion model for the self-organized aggregation of German cockroaches that includes directed movement due to an aggregation pheromone. We then propose a microscopic particle model which is set into context with the macroscopic model. Our goal is to link the macroscopic and microscopic descriptions by using the singular and the hydrodynamic limit procedures. A hybrid model related to the macroscopic and microscopic models is also proposed as a cockroach aggregation model. This hybrid model assumes that each individual responds to pheromone concentration and moves by two-mode simple symmetric random walks. It shows that even though the movement of individuals is not directed, two-mode simple symmetric random walks and effect of the pheromone result in self-organized aggregation.

1. **Introduction.** Aggregation is common in several species of insects, birds, fish, and other animals and is considered to be favorable to survival. In order to aggregate effectively, some organisms produce and respond to chemical substances called pheromones. Pheromones that are responsible for the aggregation of organisms are referred to as aggregation pheromones. (For instance [2][22].)

In this paper, we are concerned with the aggregation phenomenon of German cockroaches (*Blattela germanica*), which is well documented (see [11][12][13]). These cockroaches both secrete and detect an aggregation pheromone in order to maintain a suitable population density. Experimental evidence has shown that the movement of these cockroaches depends on the concentration of the aggregation pheromone,

2000 *Mathematics Subject Classification.* Primary: 35K55, 60K35; Secondary: 82C22, 92D25.
Key words and phrases. Cross-diffusion system, reaction-diffusion system, particle system, hydrodynamic limit, chemotaxis.

that is, if the concentration is low, they walk around actively, whereas if it is high, they become less active or remain stationary. When the concentration is at an intermediate level, their movement is not so clear, but it seems that they move towards areas of higher concentration of the pheromone ([12]).

We propose a phenomenological macroscopic model of nonlinear partial differential equations (PDEs) to describe aggregation at the population level. From experimental observation ([12]), we can assume that the population movement is due either to diffusion or to movement directed by the aggregation pheromone, depending on the pheromone concentration.

Denoting the population density of individuals by $u(t,x)$ and the pheromone concentration by $v(t,x)$ at time t and position x, we propose the following cross-diffusion system for the unknowns u and v:

$$\begin{cases} u_t = \Delta((d+\alpha H(v))u), \\ v_t = D\Delta v + au - bv, \end{cases} \quad t>0,\ x\in\Omega, \tag{1.1}$$

where d, α, D, a, and b are positive constants, and $H(v)$ is a monotonically decreasing sigmoid type function of v satisfying $0 \le H(v) \le 1$. One explicit form of $H(v)$ is

$$H(v) = \frac{1-\tanh(\gamma(v-v^*))}{2} \tag{1.2}$$

for some positive constants γ and v^*, which will be used in the numerical computations presented below. The derivation and explanation of (1.1) will be discussed in Section 2. When the equation for u in (1.1) is rewritten as

$$u_t = \mathrm{div}((d+\alpha H(v))\nabla u) + \alpha \mathrm{div}(uH'(v)\nabla v),$$

we know that the parameter α in the second term determines the strength of the directed movement. (1.1) is very close to the well known Keller-Segel model [15]:

$$\begin{cases} u_t = d\Delta u - \mathrm{div}(u\nabla\chi(v)), \\ v_t = D\Delta v + au - bv, \end{cases} \quad t>0,\ x\in\Omega,$$

which describes the aggregation dynamics of amoeba cells conducted by chemoattractant cAMP. Here the function $\chi(v)$ is a sensitivity function of v. (On the review of chemotaxis equations, see [7], [8], [9] and reference therein.)

We consider (1.1) in a bounded domain $\Omega \subset \mathbb{R}^N$ ($N \in \mathbb{N}$) with boundary conditions

$$\frac{\partial u}{\partial \nu} = \frac{\partial v}{\partial \nu} = 0, \qquad t>0,\ x\in\partial\Omega, \tag{1.3}$$

where ν is the outward-pointing unit normal vector on the smooth boundary $\partial\Omega$ and with initial conditions

$$\begin{cases} u(0,x) = u_0(x), \\ v(0,x) = v_0(x), \end{cases} \quad x\in\Omega. \tag{1.4}$$

If the parameter α in (1.1) is zero, the equation for u in (1.1) is simply reduced to the diffusion equation $u_t = d\Delta u$, so that u tends to a uniform state even if u_0 is spatially inhomogeneous. Therefore, for small α, one could expect that aggregation is never maintained (see Figure 1.1). For appropriately large α, however, Figure 1.2 indicates the occurrence of self-organized aggregation, even when the initial conditions are for an almost uniformly distributed population. This indicates that a directed movement effect is essential in order to form aggregation in (1.1). Moreover, suppose that there is a shelter at a corner in which the pheromone concentration is relatively high compared with other areas. Then, the population that was initially

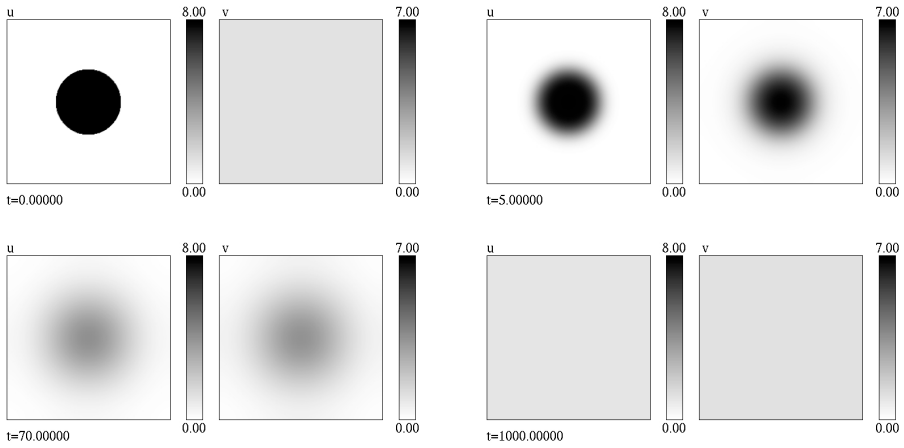

FIGURE 1.1. Snapshots of the two-dimensional pattern dynamics in (1.1), (1.3), and (1.4). The left and right figures describe u and v, respectively, at the indicated time. The parameter values and domain size are $a = b = 1$, $d = 0.005$, $\alpha = 0.00005$, $D = 0.1$, $\gamma = 20$, $v^* = 1$, and $\Omega = (0,5) \times (0,5)$.

almost uniformly distributed will eventually gather to that corner (see Figure 1.3). This numerical result qualitatively resembles the experimental observations of Ishii and Kuwahara [12].

A key question is: what kind of microscopic model is set into context with (1.1)? In order to answer this question, we derived the following reaction-diffusion system that approximates the cross-diffusion system (1.1):

$$\begin{cases} U_{1t} = d\Delta U_1 + \dfrac{1}{\varepsilon}(k(V)U_2 - h(V)U_1), \\ U_{2t} = (d+\alpha)\Delta U_2 - \dfrac{1}{\varepsilon}(k(V)U_2 - h(V)U_1), \\ V_t = D\Delta V + a(U_1 + U_2) - bV, \end{cases} \tag{1.5}$$

where $k(s)$ and $h(s)$ are respectively monotonically increasing and decreasing functions for $s \geq 0$. U_1 and U_2 are the subpopulation densities of u, which indicate the less motile and motile population densities, respectively, and convert to each other with the rates $k(V)/\varepsilon$ and $h(V)/\varepsilon$. Adding the equations for U_1 and U_2, and taking $U := U_1 + U_2$, we obtain

$$U_t = d\Delta U + \alpha\Delta U_2. \tag{1.6}$$

By letting $\varepsilon \to 0$, we can formally derive $k(V)U_2 - h(V)U_1 = 0$ from the first and second equations in (1.5) and obtain $U_2 = \frac{h(V)}{k(V)+h(V)}U$. Applying this result to (1.6), (1.1) is formally obtained under a condition $H(V) = \frac{h(V)}{h(V)+k(V)}$, so that we expect that (1.1) is approximated by (1.5) when ε is sufficiently small. The rigorous convergence of a solution of (1.5) to that of (1.1) as ε tends to zero will be shown in Sections 3 and 4.

It is well known from an experiment that each cockroach can be in two states, moving and stopped([14]). From this fact, we propose a microscopic model that

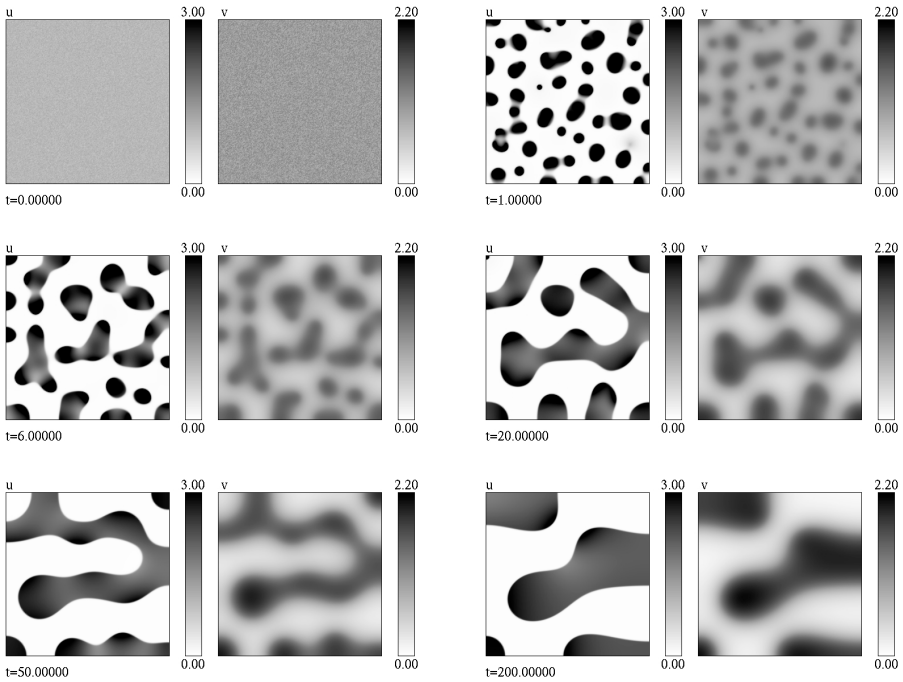

FIGURE 1.2. Snapshots of two-dimensional self-organized aggregation dynamics in (1.1), (1.3), and (1.4), where $u_0(x) \equiv 1$ and $v_0(x) \equiv 1$ with small perturbation. The left and right figures describe u and v, respectively, at the indicated time. The parameter values and domain size are $a = b = 1$, $d = 0.005$, $\alpha = 0.515$, $D = 0.1$, $\gamma = 20$, $v^* = 1$, and $\Omega = (0, 5) \times (0, 5)$.

is associated with the reaction-diffusion system (1.5). At the microscopic level, we simply represent the German cockroaches as particles. These particles can have two internal states, that is, less active (L) and active (A) states. The macroscopic population densities of particles with L and A states are given by U_1 and U_2, respectively. The evolutional law of the particle system is prescribed as follows:

(A.1) Each particle moves according to a simple symmetric random walk on an N-dimensional square lattice with a jump rate of d if it is L-type or a rate of $d + \alpha$ if it is A-type.

(A.2) Each particle secretes a diffusive chemical substance of aggregation pheromone with a constant rate a, which evaporates at a constant rate b.

(A.3) Each particle may occasionally change its state from L to A, and vice versa, with the rate of change depending on the amount of pheromone at the position where the particle is located.

After taking a diffusive scaling limit for the microscopic system, we can derive (1.5) as its macroscopic equations, at least under the periodic boundary condition. This procedure is called the hydrodynamic limit, and an important role is played by the averaging effect due to the local ergodicity. A detailed description of the

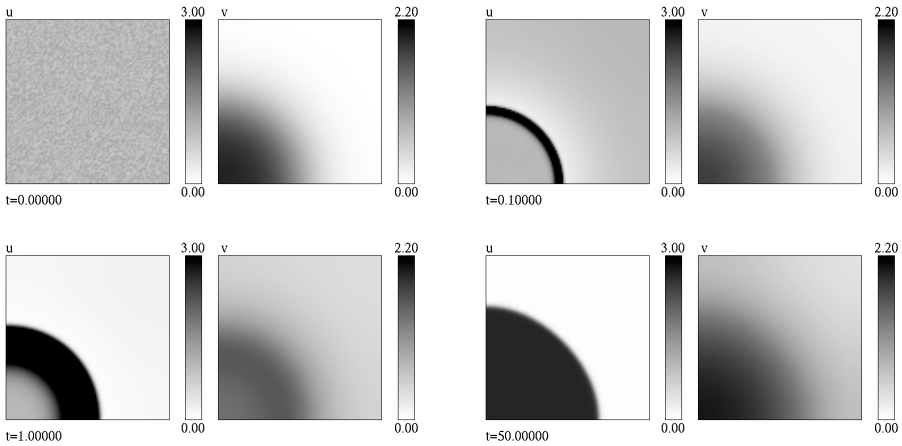

FIGURE 1.3. Snapshots of the two-dimensional pattern dynamics in (1.1), (1.3), and (1.4) when suitable pheromone concentration is initially put on a corner. The left and right figures describe u and v, respectively, at the indicated time. The parameter values and domain size are $a = b = 1$, $d = 0.005$, $\alpha = 0.515$, $D = 0.1$, $\gamma = 20$, $v^* = 1$, and $\Omega = (0, 1) \times (0, 1)$.

microscopic particle system will be presented in Section 5. Figure 1.4 shows the dynamics generated by the microscopic particle system. One can see that initially uniformly distributed cockroach particles form aggregation due to the effects of switching and pheromone as time evolves.

This paper is organized as follows: in Section 2, we propose a macroscopic cross-diffusion model including the aggregation pheromone effect introduced in Section 1. In Sections 3 and 4, we discuss the derivation of a reaction-diffusion system (1.5), and, by using the singular limit procedure as ε tends to zero, we prove that it approximates the cross-diffusion system (1.1). In Section 5, we use the hydrodynamic scaling limit procedure to prove the convergence of the microscopic particle system to the reaction-diffusion system that we introduced in Section 3. In Section 6, we propose a hybrid model related to (1.1) and the microscopic particle system, and we demonstrate with numerical simulations that it leads to self-organized aggregation. Finally, in Section 7, we present some concluding remarks on our results.

2. **A macroscopic cross-diffusion model with aggregation pheromone.**

In this section, we discuss the derivation and explanation of the macroscopic cross-diffusion model (1.1). Experimental observation indicates that if the pheromone concentration is low, individuals walk around actively, whereas if it is high, they become less active and tend to remain in the same location. At intermediate concentrations, the individuals seem to move toward the areas with a higher concentration of the pheromone([12]). We thus suppose that the population density u is phenomenologically described by the following three distinct equations, depending on

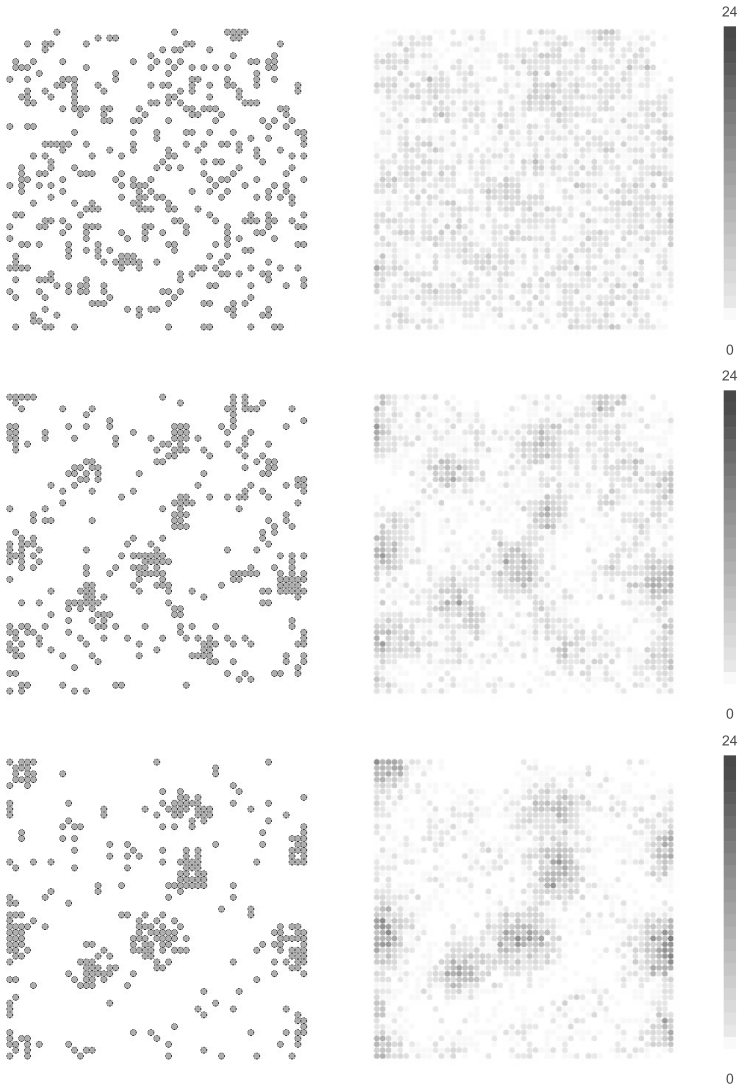

FIGURE 1.4. Snapshots of time evolution of the microscopic particle system at time 50, 1000 and 4000. The gray circles in the left and right figures denote cockroach particles and pheromone particles, respectively. The gray scale in the right figures indicates the amount of the pheromone particles. The number of the cockroach particles is 500 and the system size is $[0, 52] \times [0, 52]$.

the pheromone concentration v:

$$\begin{cases} u_t = (d+\alpha)\Delta u, & \text{if } v \text{ is small,} \\ u_t = \operatorname{div}(d_1(v)\nabla u) + \operatorname{div}(u\nabla d_2(v)), & \text{if } v \text{ is medium,} \\ u_t = d\Delta u, & \text{if } v \text{ is large,} \end{cases} \tag{2.1}$$

where d and α are positive constants, and $d_i(v)(i = 1, 2)$ are non-negative and monotonically decreasing in v. The first and third diffusion equations in (2.1) are derived from the requirement that each individual become active or less active, respectively, depending on the pheromone concentration. The second equation in (2.1) is a variation of the Keller-Segel equations that describe chemotactic movement ([15]). We assume that the diffusion rate $d_1(v)$ is approximately linearly interpolated between $d+\alpha$ and d, and, for simplicity, we assume that $d_1(v) = d_2(v)$. The second equation of (2.1) can then be rewritten as

$$u_t = \Delta(d_1(v)u), \tag{2.2}$$

which is the cross-diffusion equation that arises in mathematical ecology ([28]). If we take $d_1(v) = d + \alpha H(v)$ as a monotonically decreasing function, where $H(v)$ is a sigmoid type function of v with $0 \le H(v) \le 1$, as shown in Figure 2.1, we find that (2.1) is approximated by

$$u_t = \Delta((d + \alpha H(v))u) \quad \text{for all } v. \tag{2.3}$$

One explicit form of $H(v)$ is (1.2). The value of $H(v)$ reflects both diffusion and

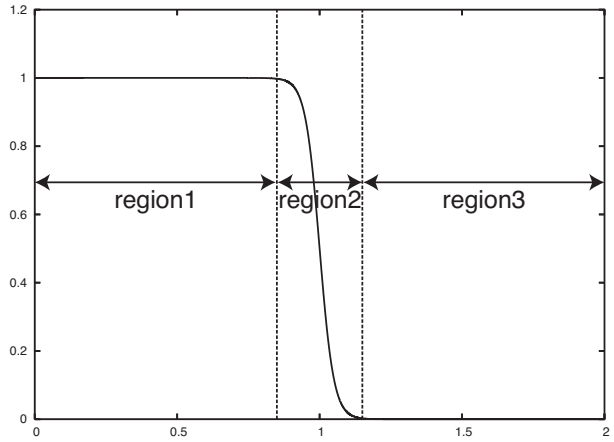

FIGURE 2.1. Function form of $H(v)$. From the profile of $H(v)$, the region is divided into three subregions, where $H(v) \approx 1$ and $H'(v) \approx 0$ for small v (region 1), $H(v) \approx 0$ and $H'(v) \approx 0$ for large v (region 3), and $0 < H(v) < 1$ and $H'(v) < 0$ for medium v (region 2).

directed movement because equation (2.3) can be decomposed into

$$u_t = \mathrm{div}((d + \alpha H(v))\nabla u) + \alpha \mathrm{div}(uH'(v)\nabla v). \tag{2.4}$$

The first term of (2.4) is a nonlinear diffusion of Fickian type, and the second one implies directed movement, depending on the gradient of v. Let us explain (2.4) more precisely. Figure 2.1 indicates that the sigmoid type function $H(v)$ is divided into three parts depending on v. For small v (region 1 in Figure 2.1), $H(v) \approx 1$ and $H'(v) \approx 0$, and for large v (region 3 in Figure 2.1), $H(v) \approx 0$ and $H'(v) \approx 0$. On the other hand, for medium v, $0 < H(v) < 1$, and $H'(v)$ is negative and not close to zero (region 2 in Figure 2.1). In other words, in the first term of (2.4), for small v, the diffusion rate is almost $d+\alpha$; conversely, for large v, the diffusion rate is nearly

d. Due to $H'(v) \approx 0$ in these regions, effect of the directed movement disappears. For medium v, however, directed movement in the second term in (2.4) is effective. We thus find that the cross-diffusion system (2.3) could approximate (2.1). We assume that (2.3) is coupled with the equation for pheromone concentration v given by

$$v_t = D\Delta v + au - bv,$$

where D is the diffusion rate of aggregation pheromone, and a and b are the secretion rate and the evaporation rate, respectively. All of the parameters are positive constants. As shown in Figure 1.2, we find that the directed movement effect due to $H(v)$ generates aggregation in a self-organized way, even if the initial distribution of u and v are almost spatially homogeneous. However, if the total population density is either small or large enough, since the amount of secreted pheromone is also small or large enough, (1.1) is approximately described by the diffusion equation, so that we may expect that aggregation does not occur. That is to say, if an average value $\frac{1}{|\Omega|}\int_\Omega u_0(x)dx = \overline{u}$ is either small or large, we expect that a constant equilibrium solution $(\overline{u}, \overline{v})$ with $\overline{v} = \frac{a}{b}\overline{u}$ of (1.1) and (1.3) is stable, while for medium $\overline{u}$, $(\overline{u}, \overline{v})$ seems to be unstable. In the next subsection, we discuss the stability of the constant equilibrium solution $(\overline{u}, \overline{v})$.

2.1. **Stationary problem in one-dimension.** In this subsection, we analyze the linear stability of the constant equilibrium solution $(\overline{u}, \frac{a}{b}\overline{u})$ that is parametrized by $\overline{u} > 0$. We consider the following one-dimensional system in a finite interval $(0, L)$:

$$\begin{cases} u_t = ((d + \alpha H(v))u)_{xx}, \\ v_t = Dv_{xx} + au - bv, \end{cases} \quad t > 0,\ x \in (0, L), \tag{2.5}$$

with zero-flux boundary conditions

$$u_x = v_x = 0, \quad t > 0,\ x = 0, L. \tag{2.6}$$

Substituting $u = \overline{u} + \tilde{u}$ and $v = \frac{a}{b}\overline{u} + \tilde{v}$ into (2.5) and neglecting higher-order terms leads to a linearized system from (2.5):

$$\begin{cases} \tilde{u}_t = (d + \alpha H(\frac{a}{b}\overline{u}))\tilde{u}_{xx} + \alpha H'(\frac{a}{b}\overline{u})\overline{u}\tilde{v}_{xx}, \\ \tilde{v}_t = D\tilde{v}_{xx} + a\tilde{u} - b\tilde{v}, \end{cases}$$

where H' implies the first derivative with respect to v. By simple calculations, we can obtain the bifurcation curves of the constant equilibrium solution $(\overline{u}, \frac{a}{b}\overline{u})$ for each of the Fourier modes. Figure 2.2 shows the stable and unstable regions of $(\overline{u}, \frac{a}{b}\overline{u})$ in the $(\overline{u}, \alpha)$-plane. Γ_n $(n = 1, 2, \cdots)$ in Figure 2.2 are defined by

$$\Gamma_n = \left\{ (\overline{u}, \alpha) \subset \mathbb{R}^2 \middle| \left(d + \alpha H(\frac{a}{b}\overline{u})\right)(D(n\pi)^2 + b) + \alpha a H'(\frac{a}{b}\overline{u})\overline{u} = 0 \right\}.$$

From Figure 2.2, we know that for a sufficiently small α, the constant equilibrium solution $(\overline{u}, \frac{a}{b}\overline{u})$ is always stable for any $\overline{u}$. This explains the numerical result as shown in Figure 1.1. However, for suitably fixed α, the stability of $(\overline{u}, \frac{a}{b}\overline{u})$ changes, depending on $\overline{u}$. For either small or large $\overline{u}$, $(\overline{u}, \frac{a}{b}\overline{u})$ is stable, while for medium $\overline{u}$, it is unstable. Such destabilization is called cross-diffusion induced instability([18]). As a consequence of the instability, non-constant equilibrium solutions bifurcate from the constant equilibrium solution branch when $\overline{u}$ is varied. By using AUTO ([4]), Figure 2.3 shows a global bifurcation diagram of the equilibrium solutions of (2.5) and (2.6). We can see from Figure 2.3 that as $\overline{u}$ increases, the branches of the non-constant equilibrium solution bifurcate from the stable trivial branch $(\overline{u}, \frac{a}{b}\overline{u})$

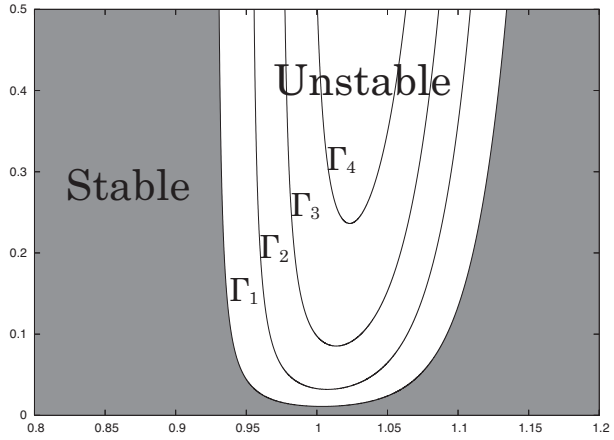

FIGURE 2.2. Stable and unstable regions for the uniform equilibrium solution $(\overline{u}, \frac{a}{b}\overline{u})$. The horizontal and vertical axes are $\overline{u}$ and α, respectively. Curves in the figure are the zero eigenvalue curves for each of the Fourier cosine modes. The parameter values are $a = b = 1$, $d = 0.05$, $D = 0.1$, $\gamma = 20$, $v^* = 1$, and $L = 1$.

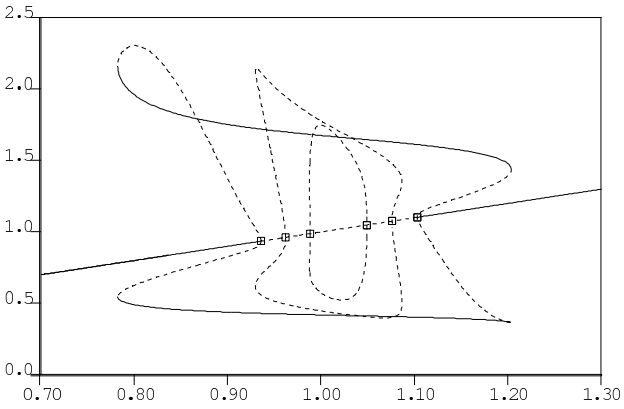

FIGURE 2.3. Bifurcation diagram of (2.5) and (2.6). The horizontal and vertical axes denote $\overline{u}$ and the value $u(x)$ at $x = 0$, respectively. The solid and dashed curves represent stable and unstable branches, respectively. The symbol $\square$ indicates the pitchfork bifurcation points. The parameter values are the same as the ones in Figure 2.2, and $\alpha = 0.15$.

through pitchfork bifurcation at approximately $\overline{u} = 0.93$. Though these nontrivial branches are unstable due to subcritical bifurcation, they become stable through saddle-node bifurcations at approximately $\overline{u} = 0.78$. Such stable non-constant equilibrium solutions exhibit self-organized aggregating patterns, as shown in Figure 2.4. From these results, we know that the self-organized aggregating patterns emerge as a

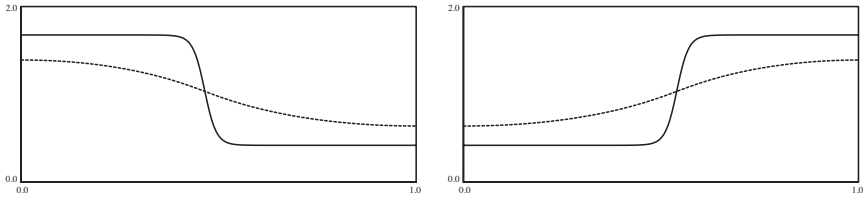

FIGURE 2.4. Profiles of stable non-constant equilibrium solutions at $\overline{u} = 1$ in Figure 2.3. The solid and dashed curves indicate u and v, respectively. The parameters are the same as the ones in Figure 2.3.

consequence of the instability of the constant equilibrium solution $(\overline{u}, \frac{a}{b}\overline{u})$. Though we have numerically obtained the global bifurcation diagram by AUTO, rigorous global bifurcation analysis of the generalized Keller-Segel model that includes (1.1) is investigated in [25].

3. **A reaction-diffusion model with aggregation pheromone.** Our goal is to propose a microscopic model which is set into context with the macroscopic cross-diffusion model (1.1). For this purpose, as a first step, we derive a reaction-diffusion system that approximates (1.1) at the macroscopic level. As mentioned above, we have seen that the function $H(v)$ possesses three parts depending on v, namely, $H(v) \approx 1$, $0 < H(v) < 1$ and $H(v) \approx 0$ for small, medium, and large v, respectively. Let us define a non-negative function $K(v)$ by $K(v) := 1 - H(v)$. We know that $K(v)$ possesses a similar property, such that $K(v) \approx 0$, $0 < K(v) < 1$, and $K(v) \approx 1$ for small, medium and large v, respectively. Then, the equation for u in (1.1) can be written as

$$\begin{aligned} u_t &= \Delta((d(K(v) + H(v)) + \alpha H(v))u) \\ &= d\Delta(K(v)u) + (d+\alpha)\Delta(H(v)u). \end{aligned}$$

Defining u_1 and u_2 as $u_1 := K(v)u$ and $u_2 := H(v)u$, u can be formally split into two subpopulation densities u_1 and u_2, with $u_1 + u_2 = u$, such that

$$(u_1 + u_2)_t = d\Delta u_1 + (d+\alpha)\Delta u_2. \tag{3.1}$$

This suggests that the cross-diffusion may be approximated by diffusion processes, and so the following reaction-diffusion system for u_1 and u_2 is considered:

$$\begin{aligned} u_{1t} &= d\Delta u_1 + F(u_1, u_2), \\ u_{2t} &= (d+\alpha)\Delta u_2 - F(u_1, u_2), \end{aligned} \tag{3.2}$$

for some suitable function $F(u_1, u_2)$. The system (3.2) implies that u is split into u_1 and u_2, which indicate less active and active population densities with some interaction between u_1 and u_2, as described by $F(u_1, u_2)$. Since $u_1 = K(v)u$, and $u_2 = H(v)u$, we obtain the relation $H(v)u_1 = K(v)u_2$. We note that this relation is achieved as a stationary state of the following system of ordinary differential equations:

$$\begin{aligned} u_{1t} &= (k(v)u_2 - h(v)u_1), \\ u_{2t} &= -(k(v)u_2 - h(v)u_1), \end{aligned} \tag{3.3}$$

provided that $H(v) = \frac{h(v)}{k(v)+h(v)}$ and $K(v) = \frac{k(v)}{h(v)+k(v)}$. The functions $h(s)$ and $k(s)$ are respectively the monotonically decreasing and increasing functions satisfying

$h(s)+k(s)\geq\mu>0$ for any $s\geq 0$, where μ is a positive constant. (3.3) indicates conversion between u_1 and u_2 depending on v. If v is low, then u_1 converts into u_2. Similarly, if v is high, then u_2 converts into u_1. If we introduce a fast time scale $\tau=\varepsilon t$ in (3.3), then (3.3) can be rewritten as

$$\begin{aligned} u_{1t}&=\frac{1}{\varepsilon}(k(v)u_2-h(v)u_1),\\ u_{2t}&=-\frac{1}{\varepsilon}(k(v)u_2-h(v)u_1), \end{aligned} \tag{3.4}$$

where we replaced τ by t again. In order to approximate the cross-diffusion system (1.1), we can combine (3.4) with (3.2) under the condition that ε is sufficiently small. Therefore, we obtain the following reaction-diffusion system with a sufficiently small parameter $\varepsilon>0$:

$$\begin{cases} U_{1t}=d\Delta U_1+\dfrac{1}{\varepsilon}(k(V)U_2-h(V)U_1),\\ U_{2t}=(d+\alpha)\Delta U_2-\dfrac{1}{\varepsilon}(k(V)U_2-h(V)U_1), & t>0,\ x\in\Omega.\\ V_t=D\Delta V+a(U_1+U_2)-bV, \end{cases} \tag{3.5}$$

Here U_1 and U_2 imply the population densities of the less active state with diffusion rate d and the active one with diffusion rate $d+\alpha$, respectively, and V represents the pheromone concentration. If V is high, U_2 changes into the less active state U_1, and if V is low, U_1 changes into the active state U_2, where $1/\varepsilon$ represents the rate of switching. We here assume that the conversion process takes place much faster than the diffusion process. One explicit forms of $h(s)$ and $k(s)$ are

$$h(s)=\frac{1-\tanh(\gamma(s-v^*))}{2}\ \text{and}\ k(s)=\frac{1+\tanh(\gamma(s-v^*))}{2} \tag{3.6}$$

for some constants γ and v^*, which will be used in the numerical computations below. In this case, since $h(s)+k(s)=1$, $H(s)$ and $K(s)$ are identical with $h(s)$ and $k(s)$, respectively. We now consider (3.5) in a bounded domain $\Omega\subset\mathbb{R}^N$ with boundary conditions

$$\frac{\partial U_1}{\partial\nu}=\frac{\partial U_2}{\partial\nu}=\frac{\partial V}{\partial\nu}=0,\qquad t>0,\ x\in\partial\Omega, \tag{3.7}$$

and initial conditions

$$\begin{cases} U_1(0,x)=U_{10}(x),\\ U_2(0,x)=U_{20}(x), & x\in\Omega.\\ V(0,x)=V_0(x), \end{cases} \tag{3.8}$$

A question then arises: let $(u_1^\varepsilon(t,x)),u_2^\varepsilon(t,x)),v^\varepsilon(t,x))$ be the solution of (3.5), (3.7), and (3.8). Does the pair of functions $(u_1^\varepsilon(t,x)+u_2^\varepsilon(t,x),v^\varepsilon(t,x))$ converge to a solution $(u(t,x),v(t,x))$ of (1.1), (1.3), and (1.4) as ε tends to zero? This question is answered by the following convergence result:

Theorem 3.1. *Arbitrarily set $T>0$. Let $(u_1^\varepsilon(t,x),u_2^\varepsilon(t,x),v^\varepsilon(t,x))$ be the solution of (3.5), (3.7), and (3.8) in $Q_T:=(0,T)\times\Omega$. There exists a weak solution $(u(t,x),v(t,x))$ of (1.1), (1.3), and (1.4) in Q_T and subsequences $\{u_1^{\varepsilon_k}\}$, $\{u_2^{\varepsilon_k}\}$, and $\{v^{\varepsilon_k}\}$ of $\{u_1^\varepsilon\}$, $\{u_2^\varepsilon\}$, and $\{v^\varepsilon\}$ such that*

$$\begin{aligned} u_1^{\varepsilon_k}+u_2^{\varepsilon_k}&\rightharpoonup u && \text{weakly in } L^2(Q_T)\\ v^{\varepsilon_k}&\to v && \text{strongly in } L^2(Q_T),\ \text{a.e. in } Q_T \text{ and}\\ & && \text{weakly in } L^2((0,T);H^1(\Omega))\cap H^1((0,T);(H^1(\Omega))') \end{aligned}$$

as $\varepsilon_k \to 0$.

This theorem will be proved in Section 4. Figure 3.1 shows the aggregation pattern generated by (3.5), (3.7), and (3.8) when ε is sufficiently small. Surprisingly, Figure

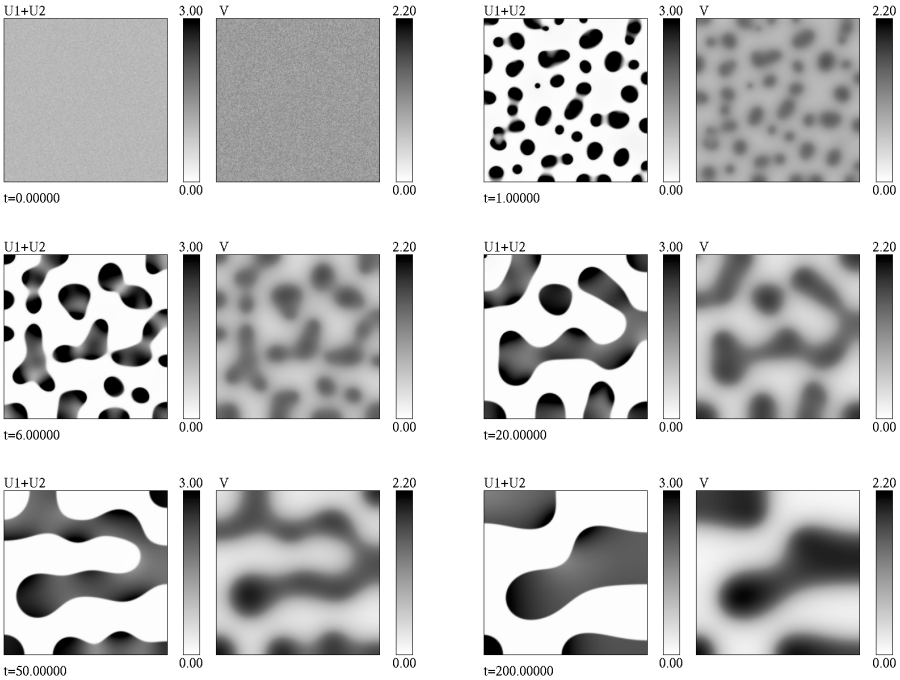

FIGURE 3.1. Snapshots of two-dimensional pattern dynamics in (3.5), (3.7), and (3.8) with $\varepsilon = 0.0001$. The initial conditions are same as the ones in Figure 1.2, where $U_{10}(x)+U_{20}(x) = u_0(x)$, and $V_0(x) = v_0(x)$ on $x \in \Omega$. The left and right figures describe U_1+U_2 and V, respectively, at the indicated time. Other parameter values and the domain size are the same as the ones in Figure 1.2.

3.1 is extremely similar to Figure 1.2 under the initial condition satisfying $U_{10} + U_{20} = u_0$ and $V_0 = v_0$, in spite of the fact that the reaction-diffusion system (3.5) no longer possesses directed movement caused by an aggregation pheromone.

The convergence theorem 3.1 holds in the finite time interval $[0, T]$. There is, however, no information on the asymptotic behavior of the solutions. In the next subsection, we will discuss both the stability of the constant equilibrium solution $\left(K(\frac{a}{b}\overline{U})\overline{U}, H(\frac{a}{b}\overline{U})\overline{U}, \frac{a}{b}\overline{U}\right)$ and the global structure of the equilibrium solutions for the one-dimensional stationary problem of the reaction-diffusion system.

3.1. **Stationary problem in one-dimension.** A constant equilibrium solution of the one-dimensional reaction-diffusion system

$$\begin{cases} U_{1t} = dU_{1xx} + \dfrac{1}{\varepsilon}(k(V)U_2 - h(V)U_1), \\ U_{2t} = (d+\alpha)U_{2xx} - \dfrac{1}{\varepsilon}(k(V)U_2 - h(V)U_1), \quad t>0,\ x\in(0,L), \\ V_t = DV_{xx} + a(U_1+U_2) - bV, \end{cases} \tag{3.9}$$

with boundary conditions

$$U_{1x} = U_{2x} = V_x = 0, \qquad t>0,\ x=0,\ L, \tag{3.10}$$

is $\left(K(\frac{a}{b}\overline{U})\overline{U}, H(\frac{a}{b}\overline{U})\overline{U}, \frac{a}{b}\overline{U}\right)$ with $K(s) = \frac{k(s)}{h(s)+k(s)}$ and $H(s) = \frac{h(s)}{h(s)+k(s)}$, parametrized by $\overline{U} := \frac{1}{L}\int_0^L (U_1+U_2)\,dx$. By a calculation similar to (2.5), we can obtain the stable and unstable regions in the $(\overline{U},\alpha)$-plane, as shown in Figure 3.2, where the bifurcation curves Γ_n $(n=1,2,\cdots)$ are defined by

$$\Gamma_n := \Big\{(\overline{U},\alpha)\subset\mathbb{R}^2 | ABC - \frac{a}{\varepsilon^2}k(\frac{a}{b}\overline{U})\eta + \frac{a}{\varepsilon^2}h(\frac{a}{b}\overline{U})\eta \\ - aB\frac{1}{\varepsilon}\eta + aA\frac{1}{\varepsilon}\eta - C\frac{1}{\varepsilon^2}h(\frac{a}{b}\overline{U})k(\frac{a}{b}\overline{U}) = 0\Big\},$$

where

$$\begin{aligned} A &= -d(n\pi)^2 - \frac{1}{\varepsilon}h(\frac{a}{b}\overline{U}), \\ B &= -(d+\alpha)(n\pi)^2 - \frac{1}{\varepsilon}k(\frac{a}{b}\overline{U}), \\ C &= -D(n\pi)^2 - b, \\ \eta &= k'(\frac{a}{b}\overline{U})H(\frac{a}{b}\overline{U})\overline{U} - h'(\frac{a}{b}\overline{U})K(\frac{a}{b}\overline{U})\overline{U}. \end{aligned}$$

We find that Figure 3.2 ($\varepsilon = 0.0001$) is quite similar to Figure 2.2. For small α, the constant equilibrium solution $\left(K(\frac{a}{b}\overline{U})\overline{U}, H(\frac{a}{b}\overline{U})\overline{U}, \frac{a}{b}\overline{U}\right)$ is stable for any $\overline{U}$. For a suitably fixed α, its stability varies according to $\overline{U}$. From the viewpoint of linear stability analysis, we can regard (3.5) as a reaction-diffusion system of the substrate-depletion type, such as the Gray-Scott model([24]) and an exothermic reaction-diffusion system([19]), where U_2 and V are viewed as fuel and temperature, respectively. We already know that these substrate-depletion systems cause Turing's diffusion-induced instability. Therefore, we can say that the cross-diffusion induced instability and Turing's diffusion-induced instability are due to similar mechanisms.

Next, by using AUTO ([4]), we produced a diagram of the global bifurcation of the equilibrium solutions of (3.9) and (3.10). The global bifurcation structure of (3.9) and (3.10) in Figure 3.3 is extremely similar to that of (2.5) and (2.6) in Figure 2.3. Stable non-constant equilibrium solutions of (3.9) and (3.10) exhibit self-organized aggregating patterns, as shown in Figure 3.4. We know that the solution profiles in Figure 3.4 resemble those in Figure 2.4. From these results, one can expect that the convergence result will also hold for the two stationary problems (2.5) and (2.6), and (3.9) and (3.10), although this is yet to be shown.

4. **Singular limit as $\varepsilon\to 0$.** In the previous section, we formally derived the three-component reaction-diffusion system (3.5) introducing subpopulation densities U_1 and U_2. It is expected that the total population density U_1+U_2 of (3.5)

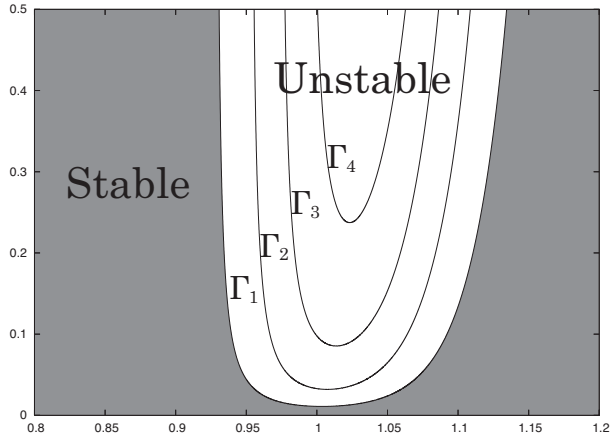

FIGURE 3.2. Stable and unstable regions for the uniform equilibrium solution $\left(K(\frac{a}{b}\overline{U})\overline{U}, H(\frac{a}{b}\overline{U})\overline{U}, \frac{a}{b}\overline{U}\right)$. The horizontal and vertical axes are $\overline{U}$ and α, respectively. Curves in the figure are the zero eigenvalue curves for each of the Fourier cosine modes. The parameter values are $a = b = 1$, $d = 0.05$, $D = 0.1$, $\gamma = 20$, $v^* = 1$, $\varepsilon = 0.0001$, and $L = 1$.

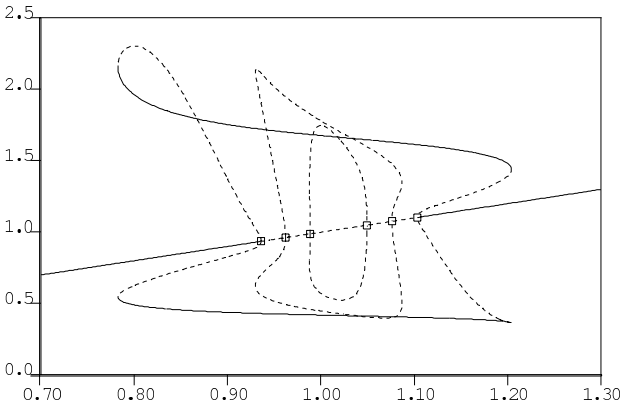

FIGURE 3.3. Bifurcation diagram of (3.5) and (3.7). The horizontal and vertical axes denote $\overline{U}$ and the value $U_1(x) + U_2(x)$ at $x = 0$, respectively. The solid and dashed curves indicate stable and unstable branches, respectively. The symbol $\square$ indicates the pitchfork bifurcation points. The parameter values are the same as the ones in Figure 3.2, and $\alpha = 0.15$.

approximates the population density u of the two-component cross-diffusion system (1.1) for sufficiently small ε. In this section, we show the convergence of the function pair $(u_1^\varepsilon + u_2^\varepsilon, v^\varepsilon)$, as ε tends to zero, which comes from an ε-parameter family of

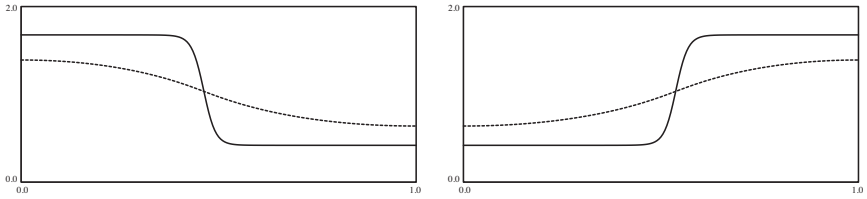

FIGURE 3.4. The profiles of stable non-constant equilibrium solutions at $\overline{U} = 1$ in Figure 3.3. The solid and dashed curves indicate $U_1 + U_2$ and V, respectively. The parameters are the same as the ones in Figure 3.3.

the three-component reaction-diffusion system

$$\begin{cases} u_{1t}^\varepsilon = d\Delta u_1^\varepsilon + \dfrac{1}{\varepsilon}(k(v^\varepsilon)u_2^\varepsilon - h(v^\varepsilon)u_1^\varepsilon), & \\ u_{2t}^\varepsilon = (d+\alpha)\Delta u_2^\varepsilon - \dfrac{1}{\varepsilon}(k(v^\varepsilon)u_2^\varepsilon - h(v^\varepsilon)u_1^\varepsilon), & t \in (0,T) \quad x \in \Omega, \\ v_t^\varepsilon = D\Delta v^\varepsilon + a(u_1^\varepsilon + u_2^\varepsilon) - bv^\varepsilon, & \\ \dfrac{\partial u_1^\varepsilon}{\partial \nu} = \dfrac{\partial u_2^\varepsilon}{\partial \nu} = \dfrac{\partial v^\varepsilon}{\partial \nu} = 0, & t \in (0,T) \quad x \in \partial\Omega, \\ u_1^\varepsilon(x,0) = u_{10}^\varepsilon(x), & \\ u_2^\varepsilon(x,0) = u_{20}^\varepsilon(x), & x \in \Omega, \\ v^\varepsilon(x,0) = v_0^\varepsilon(x), & \end{cases} \tag{4.1}$$

to a solution (u, v) of the following two-component cross-diffusion system,

$$\begin{cases} u_t = \Delta((d + \alpha H(v))u), & \\ v_t = D\Delta v + au - bv, & t \in (0,T) \quad x \in \Omega, \\ \dfrac{\partial u}{\partial \nu} = \dfrac{\partial v}{\partial \nu} = 0, & t \in (0,T) \quad x \in \partial\Omega, \\ u(x,0) = u_0 := u_{10}(x) + u_{20}(x), & \\ v(x,0) = v_0(x), & x \in \Omega, \end{cases} \tag{4.2}$$

in a rigorous way. For this purpose, we impose the following assumptions: $\{u_{10}^\varepsilon\}, \{u_{20}^\varepsilon\}$, and $\{v^\varepsilon\}$ are $C^3(\Omega)$ non-negative functions, and $u_{10}^\varepsilon \to u_{10}$, $u_{20}^\varepsilon \to u_{20}$, and $v_0^\varepsilon \to v_0$ in $L^2(\Omega)$ as $\varepsilon \to 0$. $k(s)$ and $h(s)$ are, respectively, C^2 non-negative functions satisfying $0 \le k(s), h(s) \le \xi$ and $k(s) + h(s) \ge \mu$ for $s \ge 0$, where ξ and μ are positive constants. Typical choice is (3.6).

We first affirm existence of a solution of (4.1). The proof is shown in the Appendix.

Theorem 4.1 (existence of a classical solution)**.** *We have a classical solution* $(u_1, u_2, v) \in (C^{2,1}(Q_T))^3$ *of* (4.1).

We now define a weak solution for (4.2).

Definition 4.2. We call

$$u \in L^2(Q_T)$$

and

$$v \in L^\infty((0,T); L^2(\Omega)) \cap L^2((0,T); H^1(\Omega)) \cap H^1((0,T); (H^1(\Omega))')$$

a weak solution of (4.2) if (u, v) satisfies

$$-\int\int_{Q_T} u\phi_t - \int_\Omega u_0\phi(0,\cdot) = \int\int_{Q_T} (d + \alpha H(v))u \cdot \Delta\phi$$

for any $\phi \in C^{2,1}(Q_T)$ with $\partial_x\phi \cdot \nu = 0$ on $\partial\Omega$ and $\phi(\cdot, T) = 0$ and

$$-\int\int_{Q_T} v\psi_t - \int_\Omega v_0\psi(0,\cdot) = \int\int_{Q_T} -\nabla v \cdot \nabla\psi + (au - bv)\psi$$

for any $\psi \in C^{1,1}(Q_T)$ with $\psi(\cdot, T) = 0$.

4.1. ***A priori* estimate.** Let us start the proof of a rigorous passage by using *a priori* estimates uniformly in ε.

Lemma 4.3. *Let u_1, u_2, v be solutions in $C^2(Q_T)$ of the problem (4.1). Then for all $t \in [0, T]$ and $x \in \Omega$, we have $u_1(x,t) \geq 0$,$u_2(x,t) \geq 0$, $v(x,t) \geq 0$.*

Proof. The proof follows from the maximum principle. □

Lemma 4.4 (L^2 estimate for u_1 and u_2)**.** *We have that*

$$\|u_1^\varepsilon + u_2^\varepsilon\|_{L^2(Q_T)} \leq C.$$

Moreover,

$$\|u_1^\varepsilon\|_{L^2(Q_T)} + \|u_2^\varepsilon\|_{L^2(Q_T)} \leq C,$$

where C is a positive constant.

Hereafter, let C be a generic positive constant independent of u_1, u_2, v and ε. For the proof of Lemma 4.4, we use the following lemma:

Lemma 4.5 ([1])**.** *We consider a smooth bounded subset $\Omega \subset \mathbb{R}^N$ and assume that ρ satisfies*

$$\begin{cases} \frac{\partial\rho}{\partial t} = \Delta(M(t,x)\rho) & \text{in } Q_T, \\ \frac{\partial(M\rho)}{\partial\nu} = 0 & \text{in } \partial\Omega, \\ \rho(0,x) = \rho^0(x) & \text{in } \Omega, \end{cases}$$

where M is a smooth positive function. Then for all $T > 0$,

$$\|\sqrt{M}\rho\|_{L^2(Q_T)} \leq C(\Omega)\|\rho^0\|_{L^2(\Omega)} + 2\langle\rho^0\rangle\|\sqrt{M}\|_{L^2(Q_T)},$$

where $C(\Omega)$ is the constant of Poincaré Wirtinger's inequality and $\langle\rho^0\rangle$ is the average $\frac{1}{|\Omega|}\int_\Omega \rho^0 dx$.

Proof of Lemma 4.4. Adding the first and second equations of (4.1), we obtain

$$(u_1^\varepsilon + u_2^\varepsilon)_t = \Delta(du_1^\varepsilon + (d + \alpha)u_2^\varepsilon).$$

Here for

$$0 < d \leq M := \frac{du_1^\varepsilon + (d + \alpha)u_2^\varepsilon}{u_1^\varepsilon + u_2^\varepsilon} \leq d + \alpha,$$

applying Lemma 4.5, we have

$$\|u_1^\varepsilon + u_2^\varepsilon\|_{L^2(Q_T)} \leq C(\|u_{10}^\varepsilon + u_{20}^\varepsilon\|_{L^2(\Omega)} + 1).$$

Furthermore, thanks to the non-negativity of u_1^ε and u_2^ε from Lemma 4.3, and $\|u_1^\varepsilon + u_2^\varepsilon\|_{L^2(Q_T)} \leq C$, we know that $\|u_1^\varepsilon\|_{L^2(Q_T)} \leq C$ and $\|u_2^\varepsilon\|_{L^2(Q_T)} \leq C$. □

Lemma 4.6. *We have*

$$\operatorname*{ess\,sup}_{t\in[0,T]} \int_\Omega |v^\varepsilon(t)|^2 + \int\int_{Q_T} |v^\varepsilon|^2 + \int\int_{Q_T} |\nabla v^\varepsilon|^2 \leq C.$$

Proof. Multiplying the equation for v^ε in (4.1) by v^ε, integrating over Ω, and using integration by parts, we have

$$\frac{1}{2}\frac{\partial}{\partial t}\int_\Omega |v^\varepsilon|^2 + D\int_\Omega |\nabla v^\varepsilon|^2 + b\int_\Omega |v^\varepsilon|^2 = a\int_\Omega (u_1^\varepsilon + u_2^\varepsilon)v^\varepsilon.$$

On the right-hand side, we know

$$\int_\Omega (u_1^\varepsilon + u_2^\varepsilon)v^\varepsilon \le \frac{1}{2}\int_\Omega |u_1^\varepsilon + u_2^\varepsilon|^2 + \frac{1}{2}\int_\Omega |v^\varepsilon|^2,$$

where we used the non-negativity of u_1, u_2, and v from Lemma 4.3 and Young's inequality. Combining these inequalities and integrating over $(0,T)$,

$$\begin{aligned}\frac{1}{2}\int_\Omega |v^\varepsilon(T)|^2 + D\int\int_{Q_T} |\nabla v^\varepsilon|^2 + b\int\int_{Q_T} |v^\varepsilon|^2 \\ \le C(1 + \int\int_{Q_T} |v^\varepsilon|^2)\end{aligned}$$

is obtained where we used Lemma 4.4. Thanks to the Gronwall inequality, for any $T > 0$,

$$\int_\Omega |v^\varepsilon(T)|^2 + \int\int_{Q_T} |\nabla v^\varepsilon|^2 + \int\int_{Q_T} |v^\varepsilon|^2 \le C.$$

□

Lemma 4.7. *The family $\{v_t^\varepsilon\}$ is bounded in $L^2((0,T);(H^1(\Omega))')$ uniformly with respect to ε.*

Proof. We multiply the equation for v^ε in (4.1) by $\zeta \in L^2((0,T);H^1(\Omega))$ and integrate over Q_T. Then, after integration by parts, we obtain

$$\int_0^T \langle v_t^\varepsilon, \zeta\rangle = -D\int\int_{Q^T} \nabla v^\varepsilon \cdot \nabla\zeta + \int\int_{Q_T} \{a(u_1^\varepsilon + u_2^\varepsilon) + bv^\varepsilon\}\zeta.$$

Hence from Lemmas 4.4 and 4.6, we have

$$\left|\int_0^T \langle v_t^\varepsilon, \zeta\rangle\right| \le M\|\zeta\|_{L^2((0,T);H^1(\Omega))},$$

where M is a positive constant independent of ε and ζ. If we denote the duality product between $H^1(\Omega)$ and $(H^1(\Omega))'$ by $\langle\cdot,\cdot\rangle$, we have shown that

$$\left|\int_0^T \langle v_t^\varepsilon, \zeta\rangle\right| \le M\|\zeta\|_{L^2((0,T);H^1(\Omega))}$$

for all $\zeta \in L^2((0,T);H^1(\Omega))$. This means that

$$\|v_t^\varepsilon\|_{L^2((0,T);(H^1(\Omega))')} \le M.$$

□

4.2. **Proof of Theorem 3.1.** We now prove Theorem 3.1. We deduce from Lemmas 4.4, 4.6, and 4.7 that the families $\{u_1^\varepsilon\}$, $\{u_2^\varepsilon\}$, and $\{v^\varepsilon\}$ are bounded in $L^2(Q_T)$, $L^2(Q_T)$, and $L^\infty((0,T);L^2(\Omega)) \cap L^2((0,T);H^1(\Omega)) \cap H^1((0,T);(H^1(\Omega))')$, respectively. Since $L^2((0,T);H^1(\Omega)) \cap H^1((0,T);(H^1(\Omega))')$ is precompact in $L^2(Q_T)$ (Thorem 2.1 in [29]), there exist subsequences $\{u_1^{\varepsilon_k}\}$, $\{u_2^{\varepsilon_k}\}$, and $\{v^{\varepsilon_k}\}$ of $\{u_1^\varepsilon\}$, $\{u_2^\varepsilon\}$, and $\{v^\varepsilon\}$, and functions $u_1, u_2 \in L^2(Q_T)$ and $v \in L^\infty((0,T);L^2(\Omega)) \cap L^2((0,T);H^1(\Omega)) \cap H^1((0,T);(H^1(\Omega))')$ such that

$$u_1^{\varepsilon_k} \rightharpoonup u_1, \quad u_2^{\varepsilon_k} \rightharpoonup u_2$$

weakly in $L^2(Q_T)$ and

$$v^{\varepsilon_k} \to v$$

strongly in $L^2(Q_T)$, a.e. in Q_T and weakly in $L^2((0,T);H^1(\Omega)) \cap H^1((0,T);(H^1(\Omega))')$ as $\varepsilon_k \to 0$. Therefore, we find that $k(v^{\varepsilon_k}) \to k(v)$ and $h(v^{\varepsilon_k}) \to h(v)$ strongly in $L^2(Q_T)$ and a.e. in Q_T as $\varepsilon_k \to 0$. When we multiply the equation for u_1^ε by $\varphi \in C_0^\infty(Q_T)$ and integrate over Q_T, we deduce

$$-\varepsilon \int\int_{Q_T} u_1^\varepsilon \varphi_t = \varepsilon d \int\int_{Q_T} u_1^\varepsilon \Delta\varphi + \int\int_{Q_T} \left(k(v^\varepsilon)u_2^\varepsilon - h(v^\varepsilon)u_1^\varepsilon\right)\varphi,$$

where we used integration by parts. In this expression, we take $\varepsilon_k \to 0$ along the subsequences, so that we have

$$0 = \int\int_{Q_T} \left(k(v)u_2 - h(v)u_1\right)\varphi = \int\int_{Q_T} \left(u_2(k(v)+h(v)) - h(v)(u_1+u_2)\right)\varphi$$

for all $\varphi \in C_0^\infty(Q_T)$. This means that $u_2 = \frac{h(v)(u_1+u_2)}{k(v)+h(v)}$ a.e. in Q_T. We add the equations for u_1^ε and u_2^ε, multiply by $\phi \in C^{2,1}(Q_T)$ with $\partial_x\phi \cdot \nu = 0$ on $\partial\Omega$ and $\phi(\cdot,T) = 0$, and integrate over Q_T. We then have

$$-\int\int_{Q_T} (u_1^\varepsilon + u_2^\varepsilon)\phi_t - \int_\Omega (u_{10}^\varepsilon + u_{20}^\varepsilon)\phi(\cdot,0) = \int\int_{Q_T} \left(d(u_1^\varepsilon + u_2^\varepsilon) + \alpha u_2^\varepsilon\right)\Delta\phi.$$

Letting $\varepsilon^k \to 0$ along the subsequences,

$$-\int\int_{Q_T} u\phi_t - \int_\Omega u_0\phi(\cdot,0) = \int\int_{Q_T} \left(d + \alpha\frac{h(v)}{k(v)+h(v)}\right) u\Delta\phi,$$

where we denote $u_1 + u_2$ and $u_{10} + u_{20}$ by u and u_0, respectively. Similarly, in the equation for v^ε, for any $\varphi \in C^{1,1}(Q_T)$ with $\varphi(\cdot,T) = 0$,

$$-\int\int_{Q_T} v^\varepsilon\varphi_t - \int_\Omega v_0^\varepsilon\varphi(\cdot,0) = -D\int\int_{Q_T} \nabla v^\varepsilon \cdot \nabla\varphi + (a(u_1^\varepsilon + u_2^\varepsilon) - bv^\varepsilon)\varphi.$$

Sending ε_k to zero along the subsequences, we obtain

$$-\int\int_{Q_T} v\varphi_t - \int_\Omega v_0\varphi(\cdot,0) = -D\int\int_{Q_T} \nabla v \cdot \nabla\varphi + (au - bv)\varphi.$$

We conclude the proof of Theorem 3.1.

5. **A system of weakly interacting random walks.** In the previous section, we studied the reaction-diffusion system (3.5), which is equivalent to (1.5) in Section 1. In this section, we will show that such a macroscopic system can be derived from a certain underlying microscopic system by taking a suitable space-time scaling limit that connects microscopic and macroscopic systems. Since ε is arbitrarily fixed in this section, and the factor $1/\varepsilon$ can be included in the functions h and k, we can assume $\varepsilon = 1$ without loss of generality. In the previous sections, we

imposed the zero-flux boundary condition on (3.5). However, to avoid certain technical difficulties, we will discuss the system under the periodic boundary condition instead of the Neumann boundary condition (3.7), so we take $\Omega = \mathbb{T}^N$, where $\mathbb{T}^N \equiv (\mathbb{R}/\mathbb{Z})^N (= [0,1)^N$ by identifying 1 with 0) is an N-dimensional torus.

Corresponding to the macroscopic population densities U_1 of the less active (L) state and U_2 of the active (A) state, we consider at the microscopic level families of finitely many random walks $\{X^{n,L}(t)\}_{n=1,2,\dots}$ and $\{X^{n,A}(t)\}_{n=1,2,\dots}$ moving on a discrete torus $\mathbb{T}_M^N = (\mathbb{Z}/M\mathbb{Z})^N (= \{1,2,\dots,M\}^N$ by identifying $M+1$ with 1). The ratio of the typical lengths at the macroscopic and microscopic levels is denoted by $M \in \mathbb{N}$, which plays the role of a scaling parameter, so that $\mathbb{T}_M^N$ is the (discretized) microscopic region corresponding to $\mathbb{T}^N$. Here, $X^{n,L}(t) \in \mathbb{T}_M^N$ denotes the position of the n-th L-type particle at time $t \geq 0$, while $X^{n,A}(t)$ denotes that of the n-th A-type particle. We consider random walks with continuous time t and with jump rates (jump speeds) of $X^{n,L}(t)$ and $X^{n,A}(t)$, which are given by the positive constants d_1 and d_2, respectively. Particles following these random walks move independently, but change their internal states from L to A, and vice versa, with rates that depend on the strength of the pheromone at the position where each particle is currently located. We will assume that the amount of pheromone at each site is measured by a non-negative integer at the microscopic level. The pheromone also spreads by performing independent random walks with positive rate D, and it is created proportionally to the total number of particles at each site with a constant rate a, and it evaporates with rate b.

For our purpose, it is unnecessary to distinguish particles (random walkers) by numbering them by n. We are only concerned with the number of particles with states L and A at each site $i \in \mathbb{T}_M^N$ and time $t \geq 0$, which are denoted by $\xi_i(t)$ and $\eta_i(t)$ and defined from $\{X^{n,L}(t)\}$ and $\{X^{n,A}(t)\}$ by

$$\xi_i(t) = \sum_n 1_{\{X^{n,L}(t)=i\}}, \text{ and } \eta_i(t) = \sum_n 1_{\{X^{n,A}(t)=i\}},$$

respectively.

The basic idea behind our scaling limit as $M \to \infty$ is the local average due to the so-called local ergodicity. Under the change of scales in space and time, a longer time elapses in the microscopic system compared with the macroscopic system. In fact, we introduce a diffusive scaling in time so that t at the macroscopic level is scaled to $M^2 t$ at the microscopic level. This is also true for space, namely, a small region at the macroscopic scale is enlarged by M and becomes extremely large at the microscopic scale. This yields an averaging effect in space and time for any rapid fluctuations that occur in the microscopic system, and one can replace microscopic (complex) functions by their ensemble averages. Here, the ensembles represent the equilibrium states of the family of random walks on the infinite whole lattice $\mathbb{Z}^N$, which is obtained from $\mathbb{T}_M^N$ as $M \to \infty$. Because of the conservation of particle numbers under time evolution, the equilibrium states are not unique but are parameterized by particle densities. Therefore, the averages for the microscopic system should be taken with respect to different ensembles at each corresponding location in macroscopic time and space (t,x). This kind of averaging results in a property called the local ergodicity. Note that the particles change their states from L to A, and vice versa, but that these rates are very small, and therefore this process does not change the equilibrium state. This limiting procedure is called a

hydrodynamic limit and, as a basic reference, we refer to the book of Kipnis and Landim [16].

5.1. **Microscopic system.** Let us formulate our microscopic model more precisely. Let $\mathcal{X} = \mathbb{Z}_+^{\mathbb{Z}^N}$ with $\mathbb{Z}_+ = \{0, 1, 2, \ldots\}$ be the configuration space of a particle system on $\mathbb{Z}^N$ and denote its elements by $\xi = (\xi_i)_{i\in\mathbb{Z}^N}, \eta$ or ζ. We also consider the configuration space $\mathcal{X}_M = \mathbb{Z}_+^{\mathbb{T}_M^N}$ on $\mathbb{T}_M^N$ and denote its elements by $\xi = (\xi_i)_{i\in\mathbb{T}_M^N}$ and others. For each $i \in \mathbb{Z}^N$ (or $i \in \mathbb{T}_M^N$), $\xi_i \in \mathbb{Z}_+$ represents the number of particles located at site i. We consider an operator L_0 acting on a function $f = f(\xi)$ on $\mathcal{X}$ determined by

$$L_0 f(\xi) = \sum_{i\in\mathbb{Z}^N, e\in\mathbb{Z}^N:|e|=1} \xi_i 1_{\{\xi_i\geq 1\}}\big(f(\xi^{i,i+e}) - f(\xi)\big),$$

where $\xi^{i,j} \in \mathcal{X}, i, j \in \mathbb{Z}^N$ is defined from $\xi \in \mathcal{X}$ satisfying $\xi_i \geq 1$ by

$$(\xi^{i,j})_k = \begin{cases} \xi_i - 1, & k = i, \\ \xi_j + 1, & k = j, \\ \xi_k, & k \neq i, j, \end{cases}$$

and represents the configuration obtained from ξ after one particle jumps from i to j. The operator L_0 generates a system of independent (continuous-time) simple symmetric random walks $\xi(t) = (\xi_i(t))_{i\in\mathbb{Z}^N}$ on $\mathbb{Z}^N$, which make only jumps to neighboring sites. The jump rate, which is given by ξ_i in L_0, means that each particle has the same jump rate 1. We write $1_{\{\xi_i\geq 1\}}$ in L_0 for $\xi^{i,i+e}$ to be defined, but we may actually drop it since $\xi_i = 0$ if $1_{\{\xi_i\geq 1\}} = 0$. The operator L_0 can also be defined on $\mathcal{X}_M$:

$$L_0 f(\xi) = \sum_{i\in\mathbb{T}_M^N, e\in\mathbb{Z}^N:|e|=1} \xi_i 1_{\{\xi_i\geq 1\}}\big(f(\xi^{i,i+e}) - f(\xi)\big),$$

for a function $f = f(\xi)$ on $\mathcal{X}_M$, where $i+e$ is defined in modulo M in a componentwise fashion.

Let $\mathcal{Y}_M = \mathcal{X}_M^3$, and denote its elements by (ξ, η, ζ). Consider an operator L which acts on a function $F = F(\xi, \eta, \zeta)$ on $\mathcal{Y}_M$, uses the scaling parameter M, and is determined by

$$\begin{aligned} LF(\xi,\eta,\zeta) =& d_1\{L_0F(\cdot,\eta,\zeta)\}(\xi) + d_2\{L_0F(\xi,\cdot,\zeta)\}(\eta) + D\{L_0F(\xi,\eta,\cdot)\}(\zeta) \\ &+ \frac{1}{M^2}\sum_{i\in\mathbb{T}_M^N} K(\zeta_i)\eta_i 1_{\{\eta_i\geq 1\}}\{F(\xi^{i,+},\eta^{i,-},\zeta) - F(\xi,\eta,\zeta)\} \\ &+ \frac{1}{M^2}\sum_{i\in\mathbb{T}_M^N} H(\zeta_i)\xi_i 1_{\{\xi_i\geq 1\}}\{F(\xi^{i,-},\eta^{i,+},\zeta) - F(\xi,\eta,\zeta)\} \\ &+ \frac{a}{M^2}\sum_{i\in\mathbb{T}_M^N} (\xi_i+\eta_i)\{F(\xi,\eta,\zeta^{i,+}) - F(\xi,\eta,\zeta)\} \\ &+ \frac{b}{M^2}\sum_{i\in\mathbb{T}_M^N} \zeta_i 1_{\{\zeta_i\geq 1\}}\{F(\xi,\eta,\zeta^{i,-}) - F(\xi,\eta,\zeta)\}, \end{aligned}$$

where $\xi^{i,+}$ and $\xi^{i,-} \in \mathcal{X}_M$ are defined from ξ by

$$(\xi^{i,+})_k = \begin{cases} \xi_i + 1, & k = i, \\ \xi_k, & k \neq i, \end{cases}$$

and

$$(\xi^{i,-})_k = \begin{cases} \xi_i - 1, & k = i, \\ \xi_k, & k \neq i, \end{cases}$$

respectively. These represent the configuration after the creation and annihilation of a particle at site i, respectively. Note that $\xi^{i,-}$ is defined only for configurations $\xi \in \mathcal{X}_M$ satisfying $\xi_i \geq 1$. In the definition of the operator L, d_1, d_2, D, a, and b are positive constants, and H and K are given non-negative bounded functions on $\mathbb{Z}_+$. The first term, for example, $\{L_0 F(\cdot, \eta, \zeta)\}(\xi)$, is defined by the action of L_0 on the first coordinate ξ of F.

As we explained at the beginning of this section, we have in mind a system of particles which perform independent random walks while changing their states occasionally from L to A, and vice versa. The number of particles with states L and A at site i and time t are denoted by $\xi_i(t)$ and $\eta_i(t)$, respectively, while the strength of pheromones at i, which the particles produce, is denoted by $\zeta_i(t)$. The first three terms in the generator L specify that particles with states L and A perform independent random walks with diffusive speeds d_1 and d_2 ($d_1 = d$ and $d_2 = d + \alpha$ in (3.5)), respectively, while the strength of the pheromone, taking discrete values and considered as particles, performs independent random walks with a different diffusive speed D. The fourth and fifth terms indicate that a particle changes its state from A to L, or L to A, with rates $K(\zeta_i)\eta_i/M^2$ or $H(\zeta_i)\xi_i/M^2$, respectively. Both rates are proportional to the number of particles with states A or L, but the proportional constants depend on the strength of pheromone via certain nonlinear functions K and H. The last two terms indicate that the creation of the pheromone occurs at i with rate $a(\xi_i + \eta_i)/M^2$, which is proportional to the total number of particles located at i, and annihilation occurs at i with rate $b\zeta_i/M^2$.

5.2. **Hydrodynamic scaling limit.** The (continuous-time) Markov process on $\mathcal{Y}_M$ generated by L is denoted by $(\xi(t), \eta(t), \zeta(t))$ for $t \geq 0$. We define their macroscopic density profiles $U_1^M(t,x), U_2^M(t,x)$, and $V^M(t,x)$ under the diffusive space-time scaling as

$$U_1^M(t,x) = \sum_{i \in \mathbb{T}_M^N} \xi_i(M^2 t) 1_{B^M(i/M)}(x),$$

$$U_2^M(t,x) = \sum_{i \in \mathbb{T}_M^N} \eta_i(M^2 t) 1_{B^M(i/M)}(x),$$

$$V^M(t,x) = \sum_{i \in \mathbb{T}_M^N} \zeta_i(M^2 t) 1_{B^M(i/M)}(x),$$

for $t \geq 0$ and $x \in \mathbb{T}^N$, where $B^M(i/M) := (i/M - 1/2M, i/M + 1/2M]^N$ denotes a box with center i/M and side length $1/M$. The microscopic space variable $i \in \mathbb{T}_M^N$ corresponds to the macroscopic variable $x = i/M$ by shrinking the space by M, while the microscopic time corresponding to the macroscopic t is given by $M^2 t$. This type of space-time scaling is called diffusive scaling.

We say a sequence of random functions $\{U^M \in L^1(\mathbb{T}^N)\}_{M=1,2,\ldots}$ on $\mathbb{T}^N$ converges to $U \in L^1(\mathbb{T}^N)$ as $M \to \infty$ in a weak sense in probability if

$$\lim_{M \to \infty} P(|\langle U^M - U, \varphi \rangle| > \delta) = 0$$

holds for every $\varphi \in C(\mathbb{T}^N)$ and $\delta > 0$, where $\langle U, \varphi \rangle = \int_{\mathbb{T}^N} U(x)\varphi(x)dx$. For probability measures μ_1^M and μ_2^M on $\mathcal{Y}_M$, the relative entropy of μ_1^M with respect

to μ_2^M is defined by

$$H(\mu_1^M|\mu_2^M) := \int_{\mathcal{Y}_M} \log\left(\frac{d\mu_1^M}{d\mu_2^M}(\xi,\eta,\zeta)\right) d\mu_1^M(\xi,\eta,\zeta),$$

if μ_1^M is absolutely continuous with respect to μ_2^M, and $H(\mu_1^M|\mu_2^M) = \infty$ otherwise. Then, we have the following theorem.

Theorem 5.1. *Assume that the initial values $U_1^M(0), U_2^M(0)$, and $V^M(0)$ converge to U_{10}, U_{20}, and $V_0 \in L^1(\mathbb{T}^N, [0,\infty))$, respectively, as $M \to \infty$ in a weak sense in probability. We assume two additional technical conditions on initial values: the uniform L^2-bound*

$$\sup_{M\in\mathbb{N}} E\left[\frac{1}{M^N}\sum_{i\in\mathbb{T}_M^N}\left(\xi_i(0)^2+\eta_i(0)^2+\zeta_i(0)^2\right)\right] < \infty, \tag{5.1}$$

and the boundedness of the relative entropies per volume of the distributions $\mu^M(0)$ of $(\xi(0),\eta(0),\zeta(0))$ on $\mathcal{Y}_M$ with respect to the Poisson field $\bar{\mu}_{\rho_*}^M$ on $\mathcal{Y}_M$ (see the next subsection) for some $\rho_* = (\rho_*^1,\rho_*^2,\rho_*^3)$ with $\rho_*^1,\rho_*^2,\rho_*^3 > 0$,

$$\sup_{M\in\mathbb{N}} M^{-N} H(\mu^M(0)|\bar{\mu}_{\rho_*}^M) < \infty. \tag{5.2}$$

Then, for every $t > 0$, we have the convergences

$$U_1^M(t,x) \to U_1(t,x),$$
$$U_2^M(t,x) \to U_2(t,x),$$
$$V^M(t,x) \to V(t,x),$$

as $M \to \infty$ in a weak sense in probability and the limits $U_1(t,x), U_2(t,x)$, and $V(t,x)$ are the unique weak solutions, satisfying $\sup_{0\le t\le T}\{\|U_1(t)\|_{L^1(\mathbb{T}^N)} + \|U_2(t)\|_{L^1(\mathbb{T}^N)} + \|V(t)\|_{L^1(\mathbb{T}^N)}\} < \infty$ and $\nabla U_1, \nabla U_2, \nabla V \in L^2([0,T]\times\mathbb{T}^N, \mathbb{R}^N)$ for every $T > 0$, of the following equations:

$$U_{1t} = d_1\Delta U_1 + \{k(V)U_2 - h(V)U_1\},$$
$$U_{2t} = d_2\Delta U_2 + \{h(V)U_1 - k(V)U_2\},$$
$$V_t = D\Delta V + a(U_1+U_2) - bV,$$

with initial values U_{10}, U_{20}, and V_0, where the (macroscopic) functions h and k defined for $v \ge 0$ are determined from the (microscopic) ones H and K defined on $\mathbb{Z}_+$ by

$$h(v) = E^{\mu_v}[H], \quad k(v) = E^{\mu_v}[K].$$

These are the expectations under the Poisson fields μ_v on $\mathbb{Z}^N$, which will be explained in the next subsection.

5.3. **Reversible measures for L_0.** Let μ_ρ be the Poisson fields on $\mathbb{Z}^N$ parameterized by the mean density $\rho \ge 0$, that is, μ_ρ is a probability measure on $\mathcal{X}$ such that

$$\mu_\rho(\xi_i = k) = e^{-\rho}\frac{\rho^k}{k!}\ \big(=: \nu_\rho(k)\big), \quad k \in \mathbb{Z}_+,$$

for every $i \in \mathbb{Z}^N$, and $\{\xi_i\}_{i\in\mathbb{Z}^N}$ are independent under μ_ρ, i.e., μ_ρ is a product measure of ν_ρ. Then, it is known that $\{\mu_\rho\}_{\rho\ge0}$ (and their superpositions) are

reversible and therefore invariant for L_0 defined on the whole lattice $\mathbb{Z}^N$. Indeed, a simple computation shows that

$$\begin{aligned}\sum_{k,\ell=0}^{\infty} g(k,l)\,\big[k1_{\{k\geq 1\}}\{f(k-1,\ell+1)-f(k,\ell)\}\\ +\ell 1_{\{\ell\geq 1\}}\{f(k+1,\ell-1)-f(k,\ell)\}\big]\,\nu_\rho(k)\nu_\rho(\ell)\\ =-\rho\sum_{k,\ell=0}^{\infty}\{g(k,\ell+1)-g(k+1,\ell)\}\{f(k,\ell+1)-f(k+1,\ell)\}\nu_\rho(k)\nu_\rho(\ell)\end{aligned}$$

for all bounded functions f and g on $\mathbb{Z}_+\times\mathbb{Z}_+$, and this implies the reversibility of L_0 under μ_ρ. In other words, $\{\mu_\rho\}_{\rho\geq 0}$ are the "ensembles" corresponding to the system of independent random walks on $\mathbb{Z}^d$ that are generated by L_0.

We denoted the product measure of ν_ρ on $\mathbb{T}_M^N$ by μ_ρ^M, and the product measure of the three Poisson fields $\mu_{\rho_*^1}^M$, $\mu_{\rho_*^2}^M$, and $\mu_{\rho_*^3}^M$ on $\mathbb{T}_M^N$ by $\bar\mu_{\rho_*}^M\equiv\mu_{\rho_*^1}^M\otimes\mu_{\rho_*^2}^M\otimes\mu_{\rho_*^3}^M$ with $\rho_*=(\rho_*^1,\rho_*^2,\rho_*^3)$ in Theorem 5.1.

5.4. **Proof of Theorem 5.1.** We are working on the discrete torus $\mathbb{T}_M^N$ of size M. We take a test function $\varphi\in C^\infty(\mathbb{T}^N)$ on the corresponding macroscopic torus $\mathbb{T}^N$. Then, we have that

$$\begin{aligned}\langle U_1^M(t),\varphi\rangle&=\frac{1}{M^N}\sum_{i\in\mathbb{T}_M^N}\xi_i^M(t)\bar\varphi\left(\frac{i}{M}\right),\\ \langle U_2^M(t),\varphi\rangle&=\frac{1}{M^N}\sum_{i\in\mathbb{T}_M^N}\eta_i^M(t)\bar\varphi\left(\frac{i}{M}\right),\\ \langle V^M(t),\varphi\rangle&=\frac{1}{M^N}\sum_{i\in\mathbb{T}_M^N}\zeta_i^M(t)\bar\varphi\left(\frac{i}{M}\right),\end{aligned}$$

where $\xi^M(t)=\xi(M^2t)$, $\eta^M(t)=\eta(M^2t)$, $\zeta^M(t)=\zeta(M^2t)$, and

$$\bar\varphi\left(\frac{i}{M}\right)=M^N\int_{B^M(i/M)}\varphi(x)dx.$$

Note that $\bar\varphi(i/M)$ behaves as $\varphi(i/M)$ as $M\to\infty$.

By taking the stochastic differentials, the first sum can be rewritten as

$$\begin{aligned}\langle U_1^M(t),\varphi\rangle&=\langle U_1^M(0),\varphi\rangle\\ &\quad+\frac{M^2}{M^N}\int_0^t\sum_{i\in\mathbb{T}_M^N}(L\xi_i)(\xi^M(s),\eta^M(s),\zeta^M(s))\bar\varphi\left(\frac{i}{M}\right)ds+m_1^M(t),\end{aligned}$$

where $m_1^M(t)$ is a martingale. We have similar formulas for $\langle U_2^M(t),\varphi\rangle$ and $\langle V^M(t),\varphi\rangle$. It is not difficult to see that $m_1^M(t)$ converges to 0 in the sense that

$$\lim_{M\to\infty}E[(m_1^M(t))^2]=0.$$

On the other hand, a simple computation shows that

$$\begin{aligned}L_0\xi_i&=\sum_{j\in\mathbb{T}_M^N,e\in\mathbb{Z}^N:|e|=1}\xi_j1_{\{\xi_j\geq 1\}}\big((\xi^{j,j+e})_i-\xi_i\big)\\ &=\sum_{e\in\mathbb{Z}^N:|e|=1}\big(\xi_{i-e}1_{\{\xi_{i-e}\geq 1\}}-\xi_i1_{\{\xi_i\geq 1\}}\big)=\sum_{e\in\mathbb{Z}^N:|e|=1}(\xi_{i-e}-\xi_i),\end{aligned}$$

where $j+e$ and $i-e$ are understood in modulo M. Therefore, by summation by parts,

$$\begin{aligned}\frac{M^2}{M^N}\sum_{i\in\mathbb{T}_M^N} d_1(L_0\xi_i)\bar{\varphi}\left(\frac{i}{M}\right) &= \frac{d_1M^2}{M^N}\sum_{i\in\mathbb{T}_M^N,e\in\mathbb{Z}^N:|e|=1}(\xi_{i-e}-\xi_i)\bar{\varphi}\left(\frac{i}{M}\right)\\ &= \frac{d_1}{M^N}\sum_{i\in\mathbb{T}_M^N,e\in\mathbb{Z}^N:|e|=1}\xi_i M^2\left\{\bar{\varphi}\left(\frac{i+e}{M}\right)-\bar{\varphi}\left(\frac{i}{M}\right)\right\}\\ &= \frac{d_1}{M^N}\sum_{i\in\mathbb{T}_M^N}\xi_i\left\{\Delta\varphi\left(\frac{i}{M}\right)+O\left(\frac{1}{M}\right)\right\}.\end{aligned}$$

The last equality is due to Taylor's formula. Other terms in $L\xi_i$ are computed as

$$\begin{aligned}&\frac{1}{M^2}\left\{K(\zeta_i)\eta_i 1_{\{\eta_i\geq 1\}}\left((\xi^{i,+})_i-\xi_i\right)+H(\zeta_i)\xi_i 1_{\{\xi_i\geq 1\}}\left((\xi^{i,-})_i-\xi_i\right)\right\}\\ &\quad=\frac{1}{M^2}\left\{K(\zeta_i)\eta_i-H(\zeta_i)\xi_i\right\}.\end{aligned}$$

We thus obtain that

$$\begin{aligned}\langle U_1^M(t),\varphi\rangle = \langle U_1^M(0),\varphi\rangle + \int_0^t\Bigg[&\frac{d_1}{M^N}\sum_{i\in\mathbb{T}_M^N}\xi_i^M(s)\left\{\Delta\varphi\left(\frac{i}{M}\right)+O\left(\frac{1}{M}\right)\right\}\\ &+\frac{1}{M^N}\sum_{i\in\mathbb{T}_M^N}\left\{K(\zeta_i^M(s))\eta_i^M(s)-H(\zeta_i^M(s))\xi_i^M(s)\right\}\bar{\varphi}\left(\frac{i}{M}\right)\Bigg]ds+m_1^M(t).\end{aligned}$$

The first term in the integral is approximately equal to $d_1\langle U_1^M(s),\Delta\varphi\rangle$. To study the asymptotic behavior of the second term, one needs the local ergodicity (the establishment of the local equilibrium), that is, for each i close to Mx with every fixed $x\in\mathbb{T}^N$, the distribution of $(\xi_{j+i}^M(s),\eta_{j+i}^M(s),\zeta_{j+i}^M(s))_j$ converges weakly to the product measure $\mu_{U_1(s,x)}\otimes\mu_{U_2(s,x)}\otimes\mu_{V(s,x)}$ as $M\to\infty$ (under space-time averaging) with limit functions $(U_1(s,x),U_2(s,x),V(s,x))$, which we do not know a priori. More precisely, we can show the following replacement lemma, see Lemma 1.10 in [16], p.77. We need the assumption (5.2) on the relative entropy to prove this lemma.

Lemma 5.2. *For every $\delta>0$ and $g:\mathbb{Z}_+^3\to[0,\infty)$, which grows at most linearly: $0\leq g(k_1,k_2,k_3)\leq C(k_1+k_2+k_3)$ with $C>0$, we have that*

$$\limsup_{\varepsilon\downarrow 0}\limsup_{M\to\infty}P\left(\int_0^T\frac{1}{M^N}\sum_{i\in\mathbb{T}_M^N}\tau_i G_{\varepsilon M}(\xi^M(s),\eta^M(s),\zeta^M(s))ds\geq\delta\right)=0,$$

where τ_i denote the shifts by i and for $\ell\in\mathbb{N}$

$$\begin{aligned}&G_\ell(\xi,\eta,\zeta)=\left|\frac{1}{|\Lambda_\ell|}\sum_{i\in\Lambda_\ell}g(\xi_i,\eta_i,\zeta_i)-\Phi(\xi_0^\ell,\eta_0^\ell,\zeta_0^\ell)\right|,\\ &\Lambda_\ell=[-\ell,\ell]^N\cap\mathbb{Z}^N,\quad |\Lambda_\ell|=(2\ell+1)^N,\\ &\xi_0^\ell=\frac{1}{|\Lambda_\ell|}\sum_{i\in\Lambda_\ell}\xi_i,\\ &\Phi(u_1,u_2,v)=E^{\mu_{u_1}\otimes\mu_{u_2}\otimes\mu_v}[g(\xi_0,\eta_0,\zeta_0)].\end{aligned}$$

This lemma claims that, under the space-time average, the microscopic function $g(\xi_i^M(s), \eta_i^M(s), \zeta_i^M(s))$ can be replaced by its ensemble average $\Phi(u_1, u_2, v)$ with parameters

$$u_1 = \big(\tau_i \xi_0^{\varepsilon M}\big)(\xi^M(s)) \equiv \langle U_1^M(s), \frac{1}{(2\varepsilon)^N} 1_{[-\varepsilon,\varepsilon]^N + \frac{i}{M}} \rangle,$$
$$u_2 = \big(\tau_i \eta_0^{\varepsilon M}\big)(\eta^M(s)) \equiv \langle U_2^M(s), \frac{1}{(2\varepsilon)^N} 1_{[-\varepsilon,\varepsilon]^N + \frac{i}{M}} \rangle,$$
$$v = \big(\tau_i \zeta_0^{\varepsilon M}\big)(\zeta^M(s)) \equiv \langle V^M(s), \frac{1}{(2\varepsilon)^N} 1_{[-\varepsilon,\varepsilon]^N + \frac{i}{M}} \rangle,$$

as $M \to \infty$ and then $\varepsilon \downarrow 0$.

Establishing the tightness of $\{U_1^M(t), U_2^M(t), V^M(t)\}_M$ ([16], p.71, Lemma 1.5), one gets the following identity for every limit $\{U_1(t), U_2(t), V(t)\}$ along a subsequence:

$$\langle U_1(t), \varphi \rangle = \langle U_1(0), \varphi \rangle + \int_0^t \{ d_1 \langle U_1(s), \Delta\varphi \rangle + \langle k(V(s))U_2(s) - h(V(s))U_1(s), \varphi \rangle \}\, ds,$$

by noting that

$$\int_{\mathbb{T}^N} E^{\mu_{U_1(s,x)} \otimes \mu_{U_2(s,x)} \otimes \mu_{V(s,x)}} [K(\zeta_0)\eta_0 - H(\zeta_0)\xi_0]\varphi(x)dx$$
$$= \langle k(V(s))U_2(s) - h(V(s))U_1(s), \varphi \rangle.$$

This identity is nothing but the weak and integrated form of the first equation in Theorem 5.1. We similarly get the weak form of the second equation. For the third equation, we compute terms appearing in $L\zeta_i$ as follows:

$$\frac{a}{M^2}(\xi_i + \eta_i)\big((\zeta^{i,+})_i - \zeta_i\big) + \frac{b}{M^2}\zeta_i 1_{\{\zeta_i \geq 1\}}\big((\zeta^{i,-})_i - \zeta_i\big) = \frac{a}{M^2}(\xi_i + \eta_i) - \frac{b}{M^2}\zeta_i,$$

and we have

$$\frac{1}{M^N} \int_0^t \sum_{i \in \mathbb{T}_M^N} \big\{ a(\xi_i^M(s) + \eta_i^M(s)) - b\zeta_i^M(s) \big\}\, \bar{\varphi}\left(\frac{i}{M}\right) ds$$
$$= \int_0^t \langle a(U_1^M(s) + U_2^M(s)) - bV^M(s), \varphi \rangle ds,$$

which converges to

$$\int_0^t \langle a(U_1(s) + U_2(s)) - bV(s), \varphi \rangle ds,$$

along a subsequence.

Once we can show the uniqueness of the weak solutions of the limit equations (for instance [16], p.108, Theorem 7.5), without taking subsequences, $\{U_1^M(t), U_2^M(t), V^M(t)\}_M$ themselves will be shown to converge to the unique solution. We need the assumption (5.1) to show that the limit belongs to the desired class mentioned in Theorem 5.1 to guarantee the uniqueness.

6. **A hybrid model with aggregation pheromone.** In the previous section, for a finite $\varepsilon > 0$, by using the hydrodynamic limit procedure, we showed that the reaction-diffusion system (3.5) can be derived from the microscopic particle system. Since the reaction-diffusion system (3.5) coincides with the cross-diffusion system (1.1) in the singular limit $\varepsilon \to 0$, we could make a link between the macroscopic and

microscopic descriptions. In this section, by taking into account that the conversion rates from A-type to L-type and vice versa tend to infinity (and therefore the conversion occurs rapidly), and that the size of an individual is much larger than a pheromone molecule, we propose a two-dimensional hybrid model related to (1.1) and the microscopic particle system introduced in Section 5. We then use a numerical experiment to investigate the mechanism of individual aggregation caused by aggregation pheromone.

6.1. **Description of a hybrid model.** We consider the aggregation behavior of individuals that interact with each other through the aggregation pheromone, which each individual secretes by itself, and propose a hybrid model with aggregation pheromone to describe the motion of individuals. Our model is based on the following assumptions:

(A.1) Each individual moves by a simple symmetric random walk on a square lattice. Furthermore, each individual possesses two internal states: an active state with jump rate λ^a and a less active state with jump rate λ^l.

(A.2) Each individual secretes a diffusive chemical substance, the aggregation pheromone, with a constant rate a, and this pheromone evaporates at a constant rate b.

(A.3) Each individual occasionally changes its state between active and less active, and vice versa, at a rate that depends on the local concentration of the aggregation pheromone, e.g., the individual changes its state from active to less active at a certain specified rate when the local pheromone concentration is high in its vicinity. The result is that the individual has a tendency to remain at the same site. Conversely, the individual changes its state from less active to active at a certain specified rate when the local pheromone concentration is low in its vicinity.

Based on assumptions (A.1), (A.2), and (A.3), we propose a two-dimensional hybrid model which consists of an individual-based model for individuals and a continuum model for the pheromone concentration.

We set a square domain $\overline{\Omega} := [0, L] \times [0, L]$ for $L \in \mathbb{R}^+$. Then, we define the two-dimensional square lattice with the width $l = \frac{L}{M}$ for $M \in \mathbb{N}$ on the domain $\overline{\Omega}$. We denote the two-dimensional square lattice by $S := \{0, 1, \cdots, M\} \times \{0, 1, \cdots, M\}$. We define the position of the ith individual ($i = 1, 2, \cdots, N$) at time t by $X^i(t) := (X^i_x(t), X^i_y(t)) \in S$. We also write the concentration of the aggregation pheromone as $v(t, \mathbf{x})$ at time t and position $\mathbf{x} \in \overline{\Omega}$. Let the next position $X^i(t+\tau)$ be generated by the following probabilistic procedure, where τ is the time for the motion of the individuals and should behave as $O(1/M^2)$ as $M \to \infty$ to connect to the macroscopic system. Initially, the internal state of the ith individual is decided as follows:

$$\text{the } i\text{th individual is active if } q \geq \mathscr{K}(v),$$
$$\text{the } i\text{th individual is less active if } q < \mathscr{K}(v),$$

where $\mathscr{K}(v)$ is a monotonically increasing function with $0 \leq \mathscr{K}(v) \leq 1$, and q is a pseudo-random number generated in $[0, 1]$, which is renewed at each time step and for each individual. We assume that

$$\mathscr{K}(v) = \frac{1 + \tanh(c_1 \frac{1}{|\omega^i|} \int_{\omega^i} v(t, \mathbf{x}) d\mathbf{x} - c_2)}{2},$$

where c_1 and c_2 are positive constants, and $\omega^i = [lX_x^i(t) - \frac{l}{2}, lX_x^i(t) + \frac{l}{2}] \times [lX_y^i(t) - \frac{l}{2}, lX_y^i(t) + \frac{l}{2}]$. This means that the internal state of each individual is probabilistically prescribed by the average of the local pheromone concentration. Next, the motion of individuals in active and less active states is decided as follows:

$$X^i(t+\tau) = \mathscr{P}(X^i(t), v(t,\mathbf{x})), \quad i = 1, 2, \cdots, N. \tag{6.1}$$

The operator $\mathscr{P}$ is given by

$$\mathscr{P}(X^i(t), v(t,\mathbf{x})) = \begin{cases} \mathscr{P}^a(X^i(t)), & \text{if the } i\text{th individual is active,} \\ \mathscr{P}^l(X^i(t)), & \text{if the } i\text{th individual is less active,} \end{cases}$$

where the two operators $\mathscr{P}^a$ and $\mathscr{P}^l$ correspond to active and less active states, respectively. This means that the motion is different according to the internal state of the ith individual. When the individual is active, the next position $X^i(t+\tau)$ is determined by

$$\mathscr{P}^a(X^i(t)) = \begin{cases} (X_x^i(t)+1, X_y^i(t)), & 0 \le p < \lambda^a, \\ (X_x^i(t)-1, X_y^i(t)), & \lambda^a \le p < 2\lambda^a, \\ (X_x^i(t), X_y^i(t)+1), & 2\lambda^a \le p < 3\lambda^a, \\ (X_x^i(t), X_y^i(t)-1), & 3\lambda^a \le p < 4\lambda^a, \\ (X_x^i(t), X_y^i(t)), & 4\lambda^a \le p \le 1, \end{cases}$$

where p is a pseudo-random number generated in $[0,1]$, which is renewed at each time step and for each individual. $\mathscr{P}^l$ is similarly defined by using λ^l instead of λ^a. This means that the ith individual on $X^i(t)$ moves randomly to a new position $X^i(t+\tau)$ at the next time step $t+\tau$. For the jump rates of active and less active individuals to the neighbor site, we assume the condition $0 < \lambda^l < \lambda^a \le 1/4$.

The time evolution of pheromone concentration $v(t,\mathbf{x})$ is described by a continuum model:

$$\frac{\partial v(t,\mathbf{x})}{\partial t} = D\nabla^2 v(t,\mathbf{x}) + a\sum_{i=1}^{N}\int_\Omega I_{\omega^i}(\mathbf{x})d\mathbf{x} - bv(t,\mathbf{x}), \quad t > 0 \text{ and } \mathbf{x} \in \overline{\Omega}, \tag{6.2}$$

where D is a diffusion coefficient, a and b are the secretion and evaporation rates, respectively, $I_{\omega^i}(\mathbf{x})$ is a indicator function such that

$$I_{\omega^i}(\mathbf{x}) = \begin{cases} 1, & \text{if } \mathbf{x} \in \omega^i, \\ 0, & \text{otherwise,} \end{cases}$$

and ω^i is the domain mentioned above. All of the constants are positive.

The initial position of each individual $X^i(0)$ $(i = 1, \cdots, N)$ is given at random by

$$X^i(0) = (X_x^i(0), X_y^i(0)) \quad (i = 1, \cdots, N), \tag{6.3}$$

and the initial concentration of the pheromone $v(0,\mathbf{x})$ is imposed by

$$v(0,\mathbf{x}) = 0 \quad \mathbf{x} \in \overline{\Omega}. \tag{6.4}$$

Finally, we prescribe the boundary conditions. We consider a square domain with system size $\overline{\Omega} = [0, L] \times [0, L]$ and a square lattice $S = \{0, \cdots M\} \times \{0, \cdots M\}$, with width l. Here, we assume that each individual moves on the lattice $S_{in} := \{1, \cdots M-1\} \times \{1, \cdots M-1\}$. For the position of the ith individual $X^i(t)$, the boundary condition is represented as an operator $\mathscr{B}$:

$$X^i(t+\tau) = \mathscr{B}(X^i(t), v), \quad \text{if } X^i(t) \text{ is on the boundary of } S_{in}, \tag{6.5}$$

which is similar to the operator $\mathscr{P}$ in (6.1), where

$$\mathscr{B}(X^i(t), v(t,\mathbf{x})) = \begin{cases} \mathscr{B}^a(X^i(t)), & \text{if the } i\text{th individual is active,} \\ \mathscr{B}^l(X^i(t)), & \text{if the } i\text{th individual is less active.} \end{cases}$$

The operators $\mathscr{B}^a$ and $\mathscr{B}^l$ are defined as follows: if $X^i(t) = (1, X^i_y(t))$, $X^i_y(t) \in \{2, M-2\}$ for instance, the evolution of the position of the ith individual is

$$\mathscr{B}^k(X^i(t)) = \begin{cases} (2, X^i_y(t)), & 0 \le p < \lambda^k, \\ (1, X^i_y(t)+1), & \lambda^k \le p < 2\lambda^k, \\ (1, X^i_y(t)-1), & 2\lambda^k \le p < 3\lambda^k, \\ (1, X^i_y(t)), & 3\lambda^k \le p \le 1, \end{cases}$$

where $k = a$ or l. In the same manner, we can define the boundary operators $\mathscr{B}^a$ and $\mathscr{B}^l$ for $X^i(t) = (M-1, X^i_y(t))$, $(X^i_x(t), 1)$ and $(X^i_x(t), M-1)$, $(X^i_x(t), X^i_y(t) \in \{2, 3, \cdots, M-2\})$, respectively. Moreover, when $X^i(t)$ is on the corner, that is, $X^i(t) = (1,1)$, $(1, M-1)$, $(M-1, 1)$ and $(M-1, M-1)$, the operator $\mathscr{B}^k(X^i(t))$, for example $X^i(t) = (1,1)$, is also defined by

$$\mathscr{B}^k(X^i(t)) = \begin{cases} (2,1), & 0 \le p < \lambda^k, \\ (1,2), & \lambda^k \le p < 2\lambda^k, \\ (1,1), & 2\lambda^k \le p \le 1, \end{cases}$$

where $k = a$, l. For the other corners $(1, M-1)$, $(M-1, 1)$, and $(M-1, M-1)$, the operator $\mathscr{B}$ is similarly defined. Finally, the boundary condition for v is

$$\frac{\partial v}{\partial \nu}(t, \mathbf{x}) = 0, \quad t > 0,\ \partial\Omega,$$

where ν is the outward-pointing unit normal vector.

6.2. **Numerical results.** We now present the results of the implementation of our hybrid model. We set the following parameter values for the numerical simulations: $L = 52$, $M = 52$, $l = 1$, $\lambda^a = 1/5$, $\lambda^l = 1/500$, $D = 0.5$, $a = 800$, $b = 0.1$, $c_1 = 6.25 \times 10^{-5}$, $c_2 = 1$, and $\tau = 1$. By changing the number of individuals N, we investigated the occurrence of self-organized aggregation. At first, in the case where the number of individuals was sufficiently small, almost all of the individuals moved by active random walk, which was due to the small amount of pheromone secretion. As a consequence, they did not aggregate (see Figure 6.1 for $N = 100$). In the case where the number of individuals was sufficiently large, since the pheromone concentration became high everywhere, all of the individuals changed their states from active to less active and moved by the less-active random walk. Thus, since all individuals were uniformly distributed due to the simple symmetric random walk, they again did not aggregate, as shown in Figure 6.2 for $N = 3000$. However, when the number of individuals was moderate, the situation was drastically changed, and the aggregation process of individuals was exhibited. Figure 6.3 shows that several individuals, which were initially incidentally localized, formed areas of high pheromone concentration, which triggered the generation of small clusters, which consisted of less active individuals (see Figures 6.3 (a), (b), and (c)). These clusters further developed due to repeated merging (see Figures 6.3 (c), (d), and (e)). Eventually, a few large clusters were formed (see Figures 6.3 (f)). In this aggregation process, we infer that, as time evolved, the ratio of the number of active (and less active) individuals to the number of total individuals approximately approached a

constant (see Figure 6.4). The coexistence of both active and less active individuals implies an occurrence of the self-organized aggregation of individuals. Figure 6.5 displays the ratio of the number of less active individuals to that of the total individuals when the number of the total individuals N was varied. We can see that when N increased, the ratio increased according to N. For small N, we know from Figure 6.5 that the number of less active individuals was relatively small, therefore, as was shown in Figure 6.1, clusters were not generated for small N even though some individuals stochastically changed their internal state from active to less active. On the other hand, when N was approximately 300, some clusters appeared. We can see from Figure 6.5 that the ratio of less active individuals to N drastically increased around $N = 300$. For $N > 400$, the ratio increased gradually with N. In particular, for $300 \leq N \leq 1000$, we observed the generation of clusters as shown in Figure 6.3. Finally, for large N, clusters were no longer generated as shown in Figure 6.2. In Figure 6.5, for $N = 300$, we find that the transition from a low rate of less active individuals to a high rate of less active individuals occurred as time evolved. This numerical simulation suggests that there is a tendency to take a long time to form aggregation in the neighborhood of a critical point, whether or not clusters are eventually generated. Moreover, it also takes a long time for the configuration of clusters to stabilize, even though the ratio of the number of less active individuals to that of total individuals stabilizes relatively quickly.

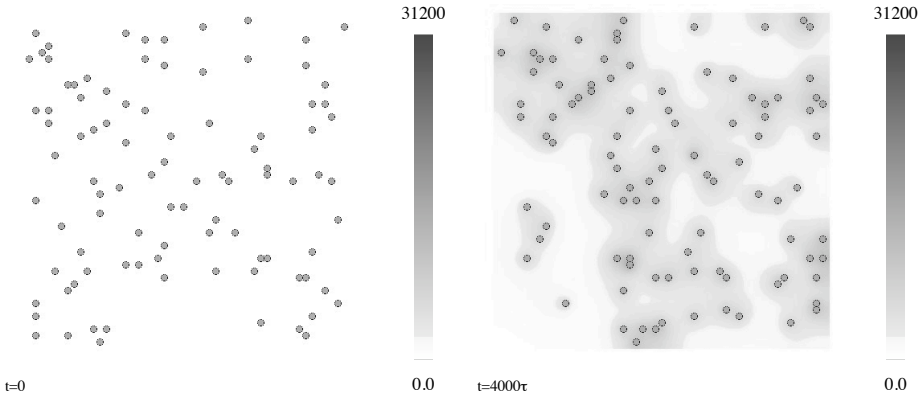

FIGURE 6.1. Snapshots of random behavior of individuals (the number is 100). The gray circles denote individuals. The gray scale in the background indicates the pheromone concentration, with black corresponding to high concentration and white corresponding to low. The system size is $[0, 52] \times [0, 52]$.

7. **Concluding remarks.** In this paper, we proposed a macroscopic cross-diffusion model that describes the aggregation phenomena of the German cockroach with aggregation pheromone. Our goal was to derive a microscopic model that is set into context with the macroscopic cross-diffusion system (1.1). In order to do that, we first introduced a reaction-diffusion system that approximated the cross-diffusion system. The reaction-diffusion approximation theory we used here was proposed by Iida, Mimura and Ninomiya [10], and Murakawa [21]. Through the reaction-diffusion system approximation, we derived a two-mode simple symmetric random

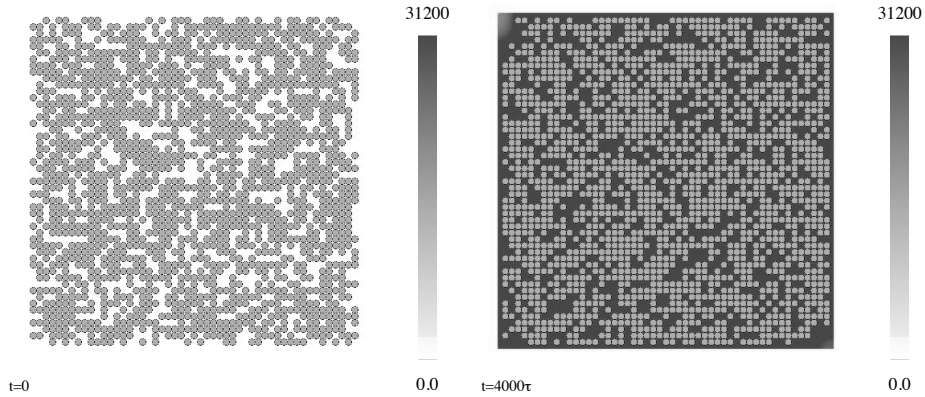

FIGURE 6.2. Snapshots of random behavior of individuals (the number is 3000). The gray circles denote individuals. The gray scale in the background indicates the pheromone concentration, with black corresponding to high concentration and white corresponding to low. The system size is $[0, 52] \times [0, 52]$.

walk particle system as a microscopic model. This microscopic model described cockroach behavior that each cockroach can be in two states, moving and stopped. Therefore, we were able to link the macroscopic and microscopic models in a rigorous way by using the singular limit and the hydrodynamic limit.

On the other hand, as a microscopic model corresponding to (1.1), we proposed a two-dimensional hybrid model which consisted of an individual-based model for the individuals and a continuum model for the pheromone concentration. This hybrid model introduced in Section 6 and can be regarded as a particle system when the conversion rate from A-type to L-type, and vice versa, tended to infinity. From the results of the numerical simulation of the hybrid model, we suggest that individuals that do not possess directed movement can nonetheless aggregate in a self-organized way by effectively using a diffusive chemical substance, although it is said that the effect of aggregation pheromones of German cockroach is still obscure([14]). However, we have not yet determined the relationship between the cross-diffusion system (1.1) and the hybrid model. The rigorous proof of that relationship is our intended area of further study. The cross-diffusion system (1.1) and the reaction-diffusion system (3.5) with growth terms are also investigated([5]). Rich aggregating pattern dynamics are exhibited in these systems.

As far as we were able to ascertain, there are several studies connecting the macroscopic population level and the microscopic individual level ([3][20][23][26][27] for instance). Connecting these two areas should provide many interesting and challenging problems for future research.

Acknowledgments. H.I. and M.M. are supported by the Meiji University Global COE Program "Formation and Development of Mathematical Sciences Based on Modeling and Analysis". C.U. is supported by the Aihara Innovative Mathematical Modelling Project, the Japan Society for the Promotion of Science (JSPS) through

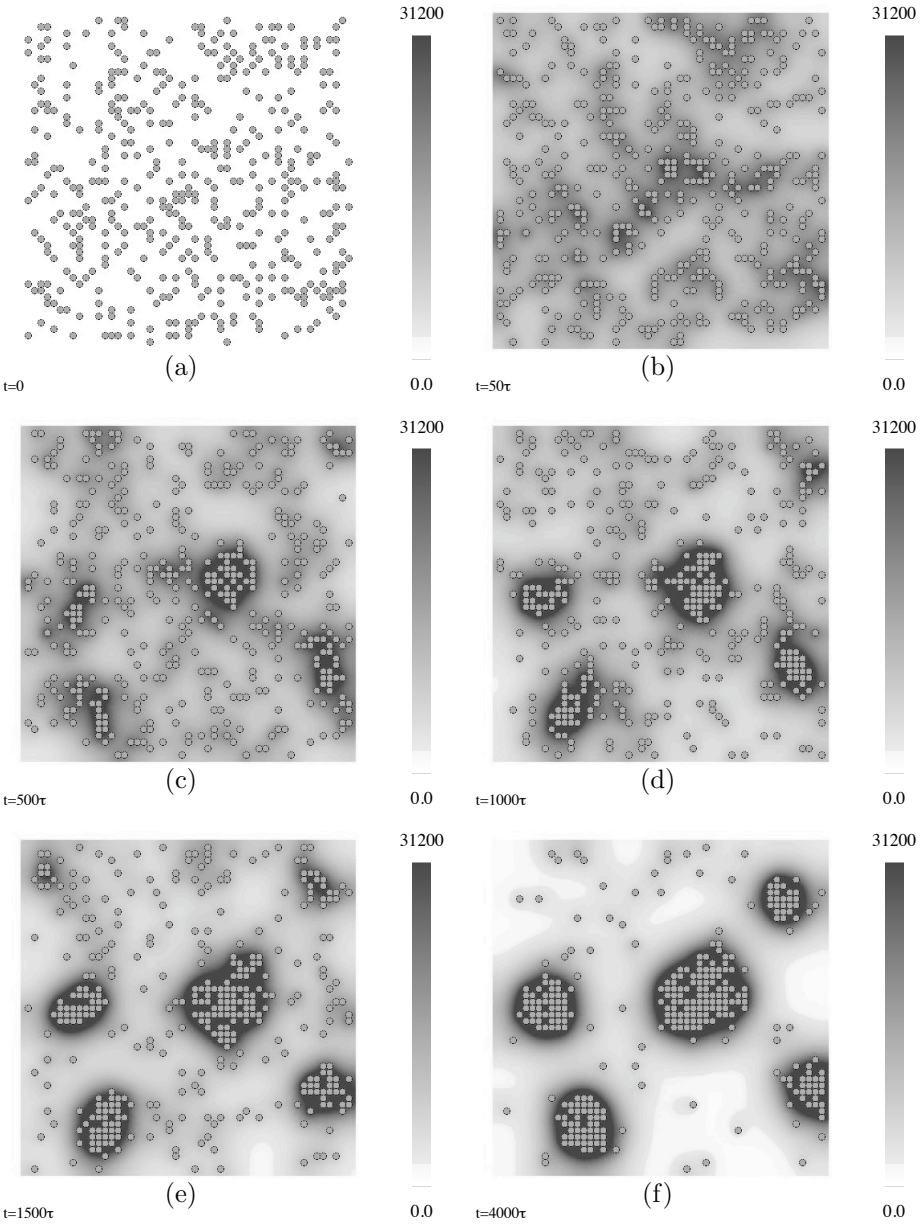

FIGURE 6.3. Snapshots of behavior of individuals (the number is 500), where τ is the unit time. The gray circles denote individuals. The gray scale in the background indicates the pheromone concentration, with black corresponding to high concentration and white corresponding to low. The system size is $[0, 52] \times [0, 52]$.

the "Funding Program for World-Leading Innovative R&D on Science and Technology (FIRST Program)", initiated by the Council for Science and Technology Policy (CSTP).

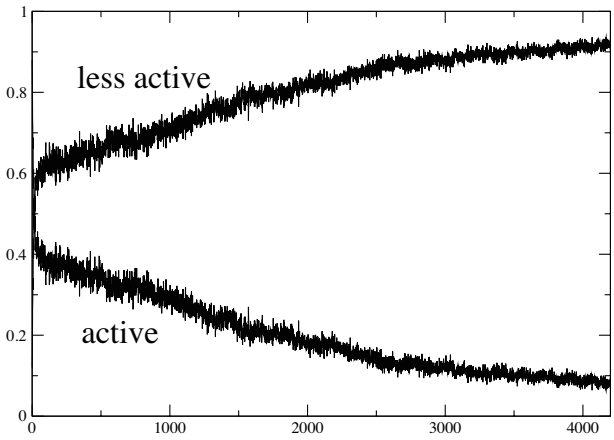

FIGURE 6.4. Time series of the ratios of active and less active individuals against the total individuals ($N = 500$). The upper curve represents the ratio for less active individuals, and the lower one is the ratio for active individuals.

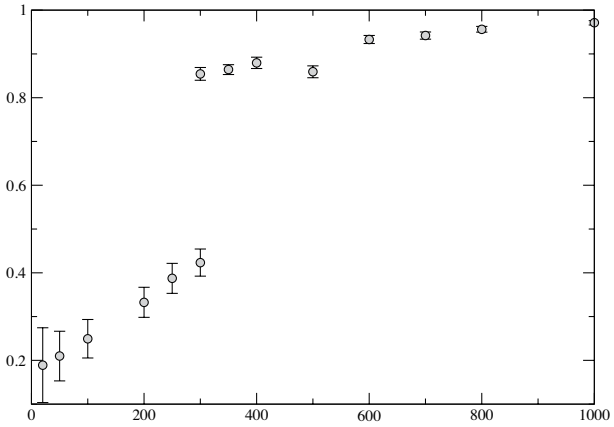

FIGURE 6.5. Dependency of the ratio of less active individuals to the number of the total individuals N. Each data point is the average of the ratio of less active individuals when the time series of the ratio is almost stable in the time interval $[t_0, t_0+2000]$, where t_0 is sufficiently large.

Appendix A. **Existence of a solution to the reaction-diffusion system.** In this appendix, we show the existence of a global solution of (A.1) as stated in

Theorem 4.1. We consider the following problem:

$$\begin{cases} u_{1t} = d\Delta u_1 + \dfrac{1}{\varepsilon}(k(v)u_2 - h(v)u_1), & \\ u_{2t} = (d+\alpha)\Delta u_2 - \dfrac{1}{\varepsilon}(k(v)u_2 - h(v)u_1), & t \in (0,T) \quad x \in \Omega, \\ v_t = D\Delta v + a(u_1+u_2) - bv, & \\ \frac{\partial u_1}{\partial \nu} = \frac{\partial u_2}{\partial \nu} = \frac{\partial v}{\partial \nu} = 0, & t \in (0,T) \quad x \in \partial\Omega, \\ u_1(x,0) = u_{10}(x), & \\ u_2(x,0) = u_{20}(x), & x \in \Omega. \\ v(x,0) = v_0(x), & \end{cases} \tag{A.1}$$

where we assume that the bounded domain $\Omega \subset \mathbb{R}^N$ with the smooth boundary $\partial\Omega$, and ν is an outward-pointing unit normal vector on the boundary. Hereinafter, we denote $\Omega \times (0,T)$ by Q_T. Moreover, we suppose that functions $h(s)$ and $k(s)$ are respectively monotonically decreasing and increasing C^2 functions such that

$$0 \le h(s), k(s) \le \xi \text{ for } s \ge 0 \text{ and } h(s) + k(s) \ge \mu > 0,$$

where ξ and μ are positive constants. A typical example is

$$k(s) = \frac{1 + \tanh(\gamma(s - v^*))}{2} \text{ and } h(s) = \frac{1 - \tanh(\gamma(s - v^*))}{2},$$

where γ and v^* are positive constants. On the initial data, we impose that

$$u_{10},\ u_{20},\ v_0 \in C^3(\overline{\Omega})$$

and are non-negative functions on $\overline{\Omega}$, respectively.

In order to prove the existence of a solution to the problem, we must obtain several a priori estimates.

Lemma A.1. *We have that*

$$\|u_1\|_{L^p(Q_T)} + \|u_2\|_{L^p(Q_T)} < C$$

for $2 \le p < \infty$.

Proof. From an estimate of the equation for u_1 ([17] Theorem 9.1 Chapter Ⅳ), we know

$$\|u_1\|_{W_2^{2,1}(Q_T)} \le C\left(\|k(v)u_2 - h(v)u_1\|_{L^2(Q_T)} + \|u_{10}\|_{L^2(\Omega)}\right).$$

Thanks to Lemma 4.4 and the boundedness of $h(s)$ and $k(s)$,

$$\|u_1\|_{W_2^{2,1}(Q_T)} \le C$$

is obtained. By the Sobolev embedding theorem, since $W_2^{2,1}(Q_T) \subset L^q(Q_T)$ with $q = \frac{2(N+2)}{N-2}$ for $N > 2$ and $2 \le q \le \infty$ for $N = 1, 2$,

$$\|u_1\|_{L^q(Q_T)} \le C.$$

Similarly, for u_2, we obtain

$$\|u_2\|_{L^q(Q_T)} \le C.$$

Repeating this procedure, we obtain the desired L^p estimate

$$\|u_1\|_{L^p(Q_T)} + \|u_2\|_{L^p(Q_T)} \le C$$

for any $p \in [2, \infty)$. □

Proof of Theorem 4.1. This proof is based on Schaefer's fixed-point theorem([6]). We fix $T > 0$ arbitrarily. For given $U_1, U_2, V \in C(\overline{Q}_T)$, consider

$$\begin{cases} u_{1t} - d\Delta u_1 = \dfrac{1}{\varepsilon}(k(V)U_2 - h(V)U_1), & \\ u_{2t} - (d+\alpha)\Delta u_2 = -\dfrac{1}{\varepsilon}(k(V)U_2 - h(V)U_1), & t \in (0,T] \quad x \in \Omega, \\ v_t - D\Delta v + bv = a(U_1 + U_2), & \\ \frac{\partial u_1}{\partial \nu} = \frac{\partial u_2}{\partial \nu} = \frac{\partial v}{\partial \nu} = 0, & t \in (0,T] \quad x \in \partial\Omega, \\ u_1(x,0) = u_{10}(x), & \\ u_2(x,0) = u_{20}(x), & x \in \Omega. \\ v(x,0) = v_0(x), & \end{cases} \tag{A.2}$$

Then from Theorem 9.1 Chapter IV [17], we obtain a unique strong solution $u_1, u_2, v \in W_p^{2,1}(Q_T)$. This mapping is denoted by P, that is $(u_1, u_2, v) = P[U_1, U_2, V]$. We define the function space

$$X = C(\overline{Q}_T).$$

Then, this mapping $P : X^3 \to X^3$ is continuos and compact. Because it follows from the Sobolev embedding theorem that $W_p^{2,1}(Q_T)$ is compactly embedded into $C^{1+\mu,(1+\mu)/2}(\overline{Q}_T)$ with $\mu \in (0, 1-(N+2)/p)$ ([17] Lemma 3.3 Chapter Ⅱ) therefore, the map $P : X^3 \to X^3$ is compact. Continuity of the map P is obvious. In order to apply Schaefer's fixed-point theorem, we must check that the set

$$\{(u_1, u_2, v) \in X^3 | (u_1, u_2, v) = \lambda P[u_1, u_2, v] \text{ for some } 0 \le \lambda \le 1\}$$

is bounded. We suppose that u_1, u_2, v is a solution of (A.1). Then, from an a priori estimate, we know that

$$\begin{aligned} \|u_1\|_{W_p^{2,1}(Q_T)} &\le C\left(\lambda \|k(v)u_2 - h(v)u_1\|_{L^p(Q_T)} + 1\right), \\ \|u_2\|_{W_p^{2,1}(Q_T)} &\le C\left(\lambda \|k(v)u_2 - h(v)u_1\|_{L^p(Q_T)} + 1\right), \\ \|v\|_{W_p^{2,1}(Q_T)} &\le C(\lambda(\|u_1\|_{L^p(Q_T)} + \|u_2\|_{L^p(Q_T)}) + 1), \end{aligned}$$

where C is a positive constant. In the left-hand side of the first and second inequalities, we can estimate

$$\|k(v)u_2 - h(v)u_1\|_{L^p(Q_T)} \le C(\|u_1\|_{L^p(Q_T)} + \|u_2\|_{L^p(Q_T)}),$$

because $0 \le h(s) \le \xi$ and $0 \le k(s) \le \xi$ for any $s \ge 0$. Thus

$$\|u_1\|_{W_p^{2,1}(Q_T)} + \|u_2\|_{W_p^{2,1}(Q_T)} + \|v\|_{W_p^{2,1}(Q_T)} \le C(\lambda(\|u_1\|_{L^p(Q_T)} + \|u_2\|_{L^p(Q_T)}) + 1).$$

Lemma A.1 gives us that

$$\|u_1\|_{W_p^{2,1}(Q_T)} + \|u_2\|_{W_p^{2,1}(Q_T)} + \|v\|_{W_p^{2,1}(Q_T)} \le C(\lambda + 1).$$

Therefore, the Sobolev embedding theorem leads to

$$\|u_1\|_X + \|u_2\|_X + \|v\|_X \le C(\lambda + 1).$$

We have performed an a priori estimate for the solution u_1, u_2, v. Applying Schaefer's fixed-point theorem, one can obtain at least one fixed point $(u_1, u_2, v) \in X^3$. Further, regularity results([17]) give us a classical solution $(u_1, u_2, v) \in (C^{2,1}(\overline{Q}_T))^3$ □

REFERENCES

[1] M. Bendahmane, T. Lepoutre, A. Marrocco and B. Perthame, *Conservative cross diffusions and pattern formation through relaxation*, J. Math. Pures Appl., **92** (2009), 651–667.

[2] S. Camazine, J.-L. Deneubourg, N. R. Franks, J. Sneyd, G. Theraulaz and E. Bonabeau, "Self-Organization in Biological Systems," Princeton University Press, Princeton, NJ, 2003.

[3] A. De Masi, S. Luckhaus and E. Presutti, *Two scales hydrodynamic limit for a model of malignant tumor cells*, Ann. Inst. H. Poincaré Probab. Statist., **43** (2007), 257–297.

[4] E. J. Doedel, R. C. Paffenroth, A. R. Champneys, T. F. Fairgrieve, Y. A. Kuznetsov, B. E. Oldeman, B. Sandstede and X. Wang, *AUTO2000: Continuation and bifurcation software for ordinary differential equations (with HomCont)*.

[5] S.-I. Ei, H. Izuhara and M. Mimura, *Infinite dimensional relaxation oscillation in aggregation-growth systems*, Discrete and Continuous Dynamical Systems, Series B, **17** (2012), 1859–1887.

[6] L. C. Evans, "Partial Differential Equations," American Mathematical Society, Providence, RI, 1998.

[7] T. Hillen and K. J. Painter, *A user's guide to PDE models for chemotaxis*, J. Math. Biol., **58** (2009), 183–217.

[8] D. Horstmann, *From 1970 until present: The Keller-Segel model in chemotaxis and its consequences. I*, Jahresber Deutsch Math., **105** (2003), 103–165.

[9] D. Horstmann, *From 1970 until present: The Keller-Segel model in chemotaxis and its consequences. II*, Jahresber Deutsch Math., **106** (2004), 51–69.

[10] M. Iida, M. Mimura and H. Ninomiya, *Diffusion, Cross-diffusion and Competitive interaction*, J. Math. Biol., **53** (2006), 617–641.

[11] S. Ishii, *An aggregation pheromone of the German cockroach, Blattella germanica (L.)*, Appl. Ent. Zool., **5** (1970), 33–41.

[12] S. Ishii and Y. Kuwahara, *An aggregation pheromone of the German cockroach Blattella germanica L. (Orthoptera: Blattelidae)*, Appl. Ent. Zool., **2** (1967), 203–217.

[13] S. Ishii and Y. Kuwahara, *Aggregation of German Cockroach (Blattella germanica) Nymphs*, Experientia, **24** (1968), 88–89.

[14] R. Jeanson, C. Rivault, J. -L. Deneubourg, S. Blanco, R. Fournier, C. Jost and G. Theraulaz, *Self-organized aggregation in cockroaches*, Animal Behavior, **69** (2005), 169–180.

[15] E. F. Keller and L. A. Segel, *Initiation of slime mold aggregation viewed as an instability*, J. Theor. Biol. **26** (1970), 399–415.

[16] C. Kipnis and C. Landim, "Scaling Limits of Interacting Particle Systems," Springer, 1999.

[17] O. A. Ladyzhenskaya, V. A. Solonnikov and N. N. Ural'ceva, "Linear and Quasilinear Equations of Parabolic Type," Transl. Math. Monographs, **23**, Amer. Math. Soc., Providence, R.I. 1967.

[18] M. Mimura and K. Kawasaki, *Spatial segregation in competitive interaction-diffusion equations*, J. Math. Biol., **9** (1980), 49–64.

[19] M. Mimura and M. Nagayama, *Nonannihilation dynamics in an exothermic reaction-diffusion system with mono-stable excitability*, Chaos, **7** (1997), 817–826.

[20] D. Morale, V. Capasso and K. Oelschläger, *An interacting particle system modeling aggregation behavior: from individuals to populations*, J. Math. Biol., **50** (2005), 49–66.

[21] H. Murakawa, *A relation between cross-diffusion and reaction-diffusion*, Discrete and Continuous Dynamical Systems, Series S, **5** (2011), 147–158.

[22] A. Okubo and S. Levin, "Diffusion and Ecological Problems: Modern Perspectives," Springer-Verlag, 2001.

[23] H. G. Othmer and A. Stevens, *Aggregation, blow up and collapse: The ABC's of taxis in reinforced random walks*, SIAM J. Appl. Math., **57** (1997), 1044–1081.

[24] J. E. Pearson, *Complex patterns in a simple system*, Science, **261** (1993), 189–192.

[25] R. Schaaf, *Stationary solutions of chemotaxis systems*, Trans. AMS, **292** (1985), 531–556.

[26] A. Stevens, *A stochastic cellular automaton modeling gliding and aggregation of myxobacteria*, SIAM J. Appl. Math., **61** (2000), 172–182.

[27] A. Stevens, *The derivation of chemotaxis equations as limit dynamics of moderately interacting stochastic many-particle systems*, SIAM J. Appl. Math., **61** (2000), 183–212.

[28] N. Shigesada, K. Kawasaki and E. Teramoto, *Spatial segregation of interacting species*, J. Theor. Biol., **79** (1979), 83–99.

[29] R. Temam, "Navier-Stokes Equations. Theory and Numerical Analysis," AMS Chelsea Publishing, Providence, RI, 2001.

Received March 2012; revised July 2012.

E-mail address: funaki@ms.u-tokyo.ac.jp
E-mail address: te08014@meiji.ac.jp
E-mail address: mimura.masayasu@gmail.com
E-mail address: chiyori@sat.t.u-tokyo.ac.jp